



# Dynamics of elastically connected double-functionally graded beam systems with different boundary conditions under action of a moving harmonic load

Mesut Şimşek<sup>a,\*</sup>, Sinan Cansız<sup>b</sup>

<sup>a</sup> Yildiz Technical University, Faculty of Civil Engineering, Department of Civil Engineering, Davutpaşa Campus, 34210 Esenler-Istanbul, Turkey

<sup>b</sup> Istanbul Aydın University, Faculty of Engineering-Architecture, Department of Civil Engineering, Florya Campus, 34295 Kucukcekmece-Istanbul, Turkey

## ARTICLE INFO

### Article history:

Available online 30 March 2012

### Keywords:

Vibration

Beam

Functionally graded beam

Elastically connected double-beam system

Moving harmonic load

## ABSTRACT

This paper studies the dynamic responses of an elastically connected double-functionally graded beam system (DFGBS) carrying a moving harmonic load at a constant speed by using Euler–Bernoulli beam theory. The two functionally graded (FG) beams are parallel and connected with each other continuously by elastic springs. Six elastically connected double-functionally graded beam systems (DFGBSs) having different boundary conditions are considered. The point constraints in the form of supports are assumed to be linear springs of large stiffness. It is assumed that the material properties follow a power-law variation through the thickness direction of the beams. The equations of motion are derived with the aid of Lagrange's equations. The unknown functions denoting the transverse deflections of DFGBS are expressed in polynomial form. Newmark method is employed to find the dynamic responses of DFGBS subjected to a concentrated moving harmonic load. The influences of the different material distribution, velocity of the moving harmonic load, forcing frequency, the rigidity of the elastic layer between the FG beams and the boundary conditions on the dynamic responses are discussed.

© 2012 Elsevier Ltd. All rights reserved.

## 1. Introduction

The concept of functionally graded materials (FGMs) was first introduced in 1984 as ultrahigh temperature-resistant materials for aircrafts, space vehicles, nuclear and other engineering applications. Since then, FGMs have attracted much interest as heat-resistant materials. Functionally graded materials are heterogeneous composite materials, in which the material properties vary continuously from one interface to the other. This is achieved by gradually varying the volume fraction of the constituent materials. The continuity of the material properties reduces the influence of the presence of interfaces and avoids high interfacial stresses. The outcome of this is that this class of materials can survive environments with high-temperature gradients, while maintaining the desired structural integrity. Investigations on the dynamic characteristics of FG structures have been an area of intensive research over the last decade (see Refs. [1–23]).

The dynamic response of beam-type structures to moving loads has been well documented in hundreds of contributions during the past few decades, owing to their extensive use in many engineering applications, such as bridges, guideways, railroads, overhead cranes and gun-tubes. Under the action of a moving load or mass, a beam-type structure produces larger deflections and higher

stresses than it does under an equivalent load applied statically. Such a structure is very important in engineering applications, especially in transportation system and in the design of machining process. Numerous previous studies have been reported in this field [24–40]. However, most of the published papers related to moving load problems are given for homogeneous beams, and research efforts devoted to vibration of FG beams under moving loads are very limited. For example, Yang et al. [41] studied free and forced vibrations of cracked FG beams subjected to an axial force and a moving load were investigated by using the modal expansion technique. Şimşek and Kocatürk [42] investigated the free and forced vibration characteristics of a FG Euler–Bernoulli beam under a moving harmonic load. Khalili et al. [43] employed the Rayleigh–Ritz method in space domain and a step-by-step differential quadrature method in time domain to study the transient response of FG beams induced by moving loads. Şimşek [44] examined dynamic deflections and stresses of an FG simply-supported beam subjected to a moving mass in the context of Euler–Bernoulli, Timoshenko and the third order shear deformation beam theories. Şimşek [45] performed the non-linear dynamic analysis of a functionally graded beam with immovable supports under a moving harmonic load. In a recent study, Yan et al. [46] studied the dynamic responses of FG Timoshenko beam with an open edge crack resting on an elastic foundation subjected to a transverse load moving at a constant speed.

A double-beam system, which consists of two parallel beams joined by innumerable coupling elastic springs and dashpots, have

\* Corresponding author. Tel.: +90 2123835146; fax: +90 2123835102.

E-mail addresses: [msimsek@yildiz.edu.tr](mailto:msimsek@yildiz.edu.tr), [mesutsimsek@gmail.com](mailto:mesutsimsek@gmail.com) (M. Şimşek).

a great importance in many fields of civil and mechanical engineering. Recently, the double-beam system has been used as a new vibration absorber to control the vibration of a beam-type structure. Such a system for vibration isolation is called as a continuous dynamic vibration absorber (CDVA) [47] or dynamic absorbing beam system (DABS) [48]. A dynamic absorbing beam system (DABS) consists of a main beam, a dynamic absorbing beam and uniformly distributed-connecting springs and dampers between the main and dynamic absorbing beam [48]. The dynamic absorbing beam and viscoelastic layer between the beams are designed in order to reduce the vibration experienced by the main beam. The double-beam system is used to model floating-slab tracks, which are widely used to control vibration from underground trains [49]. In a system of the floating-slab tracks, an upper beam accounts for the rail and a lower beam corresponds to the floating slab. Railpads between the upper and the lower beams are represented by a continuous layer of springs and dashpots. In this context, Shamalta and Metrikine [50] investigated the steady-state dynamic response of an embedded railway track to a moving train. The model for the track consists of a flexible plate performing vertical vibrations, two beams that are connected to the plate by continuous viscoelastic elements and an elastic foundation that supports the plate. Further, elastically connected concentric beams are able to capture to mechanical behavior of multi-walled carbon nanotubes in nanomechanics. The elastic layers provide a linear model for inter-atomic Van der Waals forces [51]. Because of the great practical importance in the fields of aerospace, civil and mechanical engineering, the different problems associated with the free and forced vibration analysis of the elastically connected parallel-beam systems have been investigated by several researchers. For instance, free vibration analysis of two parallel simply supported beams continuously joined by a Winkler elastic layer was presented by Oniszczuk [47]. Seelig and Hoppmann [52] studied free vibration of a system of  $n$  elastically connected parallel beams with various boundary conditions. In [52], frequencies obtained from theoretical analysis were compared with those obtained from experiment. It was concluded that for the lower modes, at least up to the eighth, the agreement between the theory and experiment was very good. Kessel [53] derived the resonance conditions for an elastically connected simply-supported double-beam system in which one of the members is subjected to a moving point load that oscillates longitudinally along the beam about a fixed point along the length of one of the beams. Rao [54] examined free flexural vibration of elastically connected Timoshenko beams considering the effects of the shear deformation and the rotary inertia. Chonan [55] studied the dynamical behavior of two identical beams connected with a set of independent springs subjected to an impulsive load by using Laplace transformations. Vu et al. [56] presented an exact method for solving the vibration of a double-beam system subject to harmonic excitation. Oniszczuk [57] investigated undamped forced transverse vibrations of an elastically connected complex simply supported double-beam system. The problem was formulated and solved in the case of simply supported beams. The classical modal expansion method was applied to ascertain dynamic responses of beams due to arbitrarily distributed continuous loads. Several cases of particularly interesting excitation loadings were investigated. The dynamic response for a simply supported homogeneous isotropic double-beam system subject to a moving constant load was investigated by Abu-Hilal [58]. Zhang et al. [59] studied the free vibration and buckling of an elastically connected simply-supported double-beam system under compressive axial loading on the basis of the Bernoulli–Euler beam theory. Based on Bernoulli–Euler beam theory, the effect of compressive axial load on the properties of forced transverse vibration of an elastically connected double-beam system was investigated by Zhang et al. [60]. In this study, two different load-

ing conditions, uniformly distributed harmonic load and a concentrated harmonic force applied at the midspan of the beam, were taken into account. Jun and Hongxing [61] developed an exact dynamic stiffness method for predicting the free vibration characteristics of a three-beam system, which is composed of three non-identical uniform beams of equal length connected by innumerable coupling springs and dashpots. On the basis of Timoshenko beam theory, Jun et al. [62] established an exact dynamic stiffness matrix for an elastically connected three-beam system, which is composed of three parallel beams of uniform properties with uniformly distributed-connecting springs among them. Ariaei et al. [63] investigated the dynamic behavior of  $n$  parallel identical elastically connected Timoshenko beam subjected to a moving load with constant magnitude. In this study, in order to decouple the governing equations, each beam was divided into  $m + 1$  segments, which are separated by  $m$  intermediate connections. It leads to discontinuities at each spring location in shear force proportional to vertical displacement. In a recent study, Şimşek [64] have presented an analytical method for the forced vibration of an elastically connected double-carbon nanotube system (DCNTS) carrying a moving nanoparticle based on the nonlocal elasticity theory. A novel state-space form for studying transverse vibrations of double-beam systems, made of two outer elastic beams continuously joined by an inner viscoelastic layer, has been presented by Palmeri and Adhikari [65].

The above review clearly indicates that the majority of the aforementioned works on the elastically connected beams are related to the free vibration analysis of beams made of homogeneous material properties. Further, the works [53,57,58,63,64] related to the forced vibration of double-beam systems subjected to moving loads were limited to the particular cases of identical beams with simply-supported boundary conditions, homogeneous material properties. Also, in these works, the moving load is not harmonic, namely it is a moving load with constant magnitude. Because, the title problem with arbitrary boundary conditions and forcing functions is difficult to solve. Under certain conditions, the problem becomes tractable. Also, closed-form solutions for the forced response of damped double-beam systems can be obtained under specialized cases. The present formulation is very useful to analyze double or multiple-beam system with arbitrary forcing function and arbitrary boundary conditions including elastic support, multiple-beam system whose elements are made of different material composition, those with variable cross-section etc. The dynamic responses of the elastically connected functionally graded double-beam system (DFGBS) with the different boundary conditions of the two parallel beams to a moving harmonic load are not available in the open literature.

Therefore, based on the above discussion there is a strong encouragement to gain an understanding of the entire subject of vibration complex beam system and the mathematical modeling of such phenomena. This paper focuses on the dynamic behavior of DFGBS subjected to a moving harmonic load at a constant speed based on Euler–Bernoulli beam theory. The two parallel functionally graded (FG) beams are connected with each other continuously by elastic springs. Six elastically connected double-functionally graded beam systems (DFGBSs) having different boundary conditions, which are combination of pinned, clamped and free end supports, are considered. The point constraints of the supports are modeled as linear springs of very large stiffness. These linear springs of sufficiently large stiffness will ensure that the points where the springs attached will remain stationary during the transverse deformation of the beam. Material properties of the beams vary continuously in the thickness direction according to the power-law form. The equations of motion are derived with the aid of Lagrange's equations. The unknown functions denoting the transverse deflections of DFGBS are expressed in polynomial form.

Newmark method [66] is employed to find the dynamic responses of DFGBS subjected to a concentrated moving harmonic load. The influences of the different material distribution, velocity of the moving harmonic load, forcing frequency, the rigidity of the elastic layer between the FG beams and the boundary conditions on the dynamic responses are discussed.

**2. Theory and formulations**

The physical model of the DFGBS under consideration is composed of two parallel, slender, prismatic and functionally graded beams connected each other by innumerable coupling springs with the spring constant  $k_w$ , as shown in Fig. 1. The beams are supported with the aid of the elastic springs of very large stiffness at the end of the beams. All beams have the same length  $L$ , width  $b$ , thickness  $h$ . The top and the bottom beams are designated as the primary beam and the secondary beam, respectively. The primary beam is subjected to a moving harmonic load  $Q(t)$ , which moves in the axial direction of the beam with constant velocity,  $v_Q$ . It is assumed that the moving harmonic load is in contact with the primary beam during the excitation, and the inertial effects of the moving load are negligible.

In this study, it is assumed that material properties of the beam, i.e., Young’s modulus  $E$  and mass density  $\rho$ , vary continuously in the thickness direction ( $z$  axis) according to the power-law form. Therefore, the material properties are the functions of the  $z$  coordinate, namely  $E = E(z)$  and  $\rho = \rho(z)$ . According to the rule of mixture, the effective material property,  $P$ , can be expressed as

$$P = P_T V_T + P_B V_B \tag{1}$$

where  $P_T$  and  $P_B$  are the material properties of the top and the bottom surfaces of the beam,  $V_T$  and  $V_B$  are the volume fractions of the top and bottom surfaces of the beam and related by

$$V_T + V_B = 1 \tag{2}$$

The effective material properties of the FG beam is defined by the power-law form introduced by [67]. The volume fraction of the upper constituent of the beam is assumed to be given by

$$V_T = \left(\frac{z}{h} + \frac{1}{2}\right)^k \tag{3}$$

where  $k$  is the power-law exponent which dictates the material variation profile through the thickness of the beam. Fig. 2 shows variation of the volume fraction of the upper constituent,  $V_T$ , through the thickness of the beam.

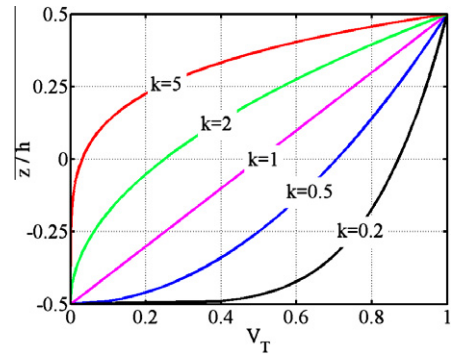


Fig. 2. Variation of the volume fraction of the upper constituent,  $V_T$ , through the thickness of the FG beams.

Therefore, from Eqs. (1)–(3), the effective Young’s modulus  $E$  and the effective mass density  $\rho$  of the FG beam can be expressed as follows:

$$E(z) = (E_T - E_B) \left(\frac{z}{h} + \frac{1}{2}\right)^k + E_B \tag{4a}$$

$$\rho(z) = (\rho_T - \rho_B) \left(\frac{z}{h} + \frac{1}{2}\right)^k + \rho_B \tag{4b}$$

It is evident from Eqs. (4a–b) that when  $z = -h/2$ ,  $E = E_B$ ,  $\rho = \rho_B$  and when  $z = h/2$ ,  $E = E_T$ ,  $\rho = \rho_T$ . Considering the small deformations and assuming the material of FG beam obeys Hooke’s law, the internal strain energy of DFGBS based on the Euler–Bernoulli beam theory is given as

$$U_{int} = \frac{1}{2} \sum_{i=1}^2 \left\{ \int_{-L/2}^{L/2} \left[ A_{xx} \left(\frac{\partial u_i(x,t)}{\partial x}\right)^2 - 2B_{xx} \left(\frac{\partial u_i(x,t)}{\partial x}\right) \left(\frac{\partial^2 w_i(x,t)}{\partial x^2}\right) + D_{xx} \left(\frac{\partial^2 w_i(x,t)}{\partial x^2}\right)^2 \right] dx \right\} \tag{5}$$

where subscripts  $i = 1, 2$  denote the primary and the secondary beams, respectively.  $u_i$  and  $w_i$  are the axial and the transverse displacements of the  $i$ th beam,  $x$  is the spatial co-ordinate and  $t$  denotes time.  $A_{xx}$ ,  $B_{xx}$  and  $D_{xx}$  are extensional, coupling and bending rigidities, respectively and defined as follows:

$$(A_{xx}, B_{xx}, D_{xx}) = \int_A E(z)(1, z, z^2) dA \tag{6}$$

Potential energy induced by the elastic layer between the beams is given as

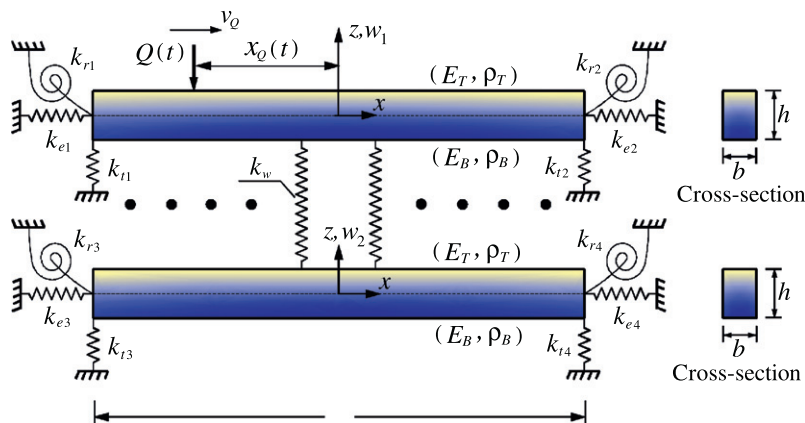


Fig. 1. An elastically connected double-functionally graded beam system (DFGBS) subjected to a concentrated moving harmonic load.

$$U_{el} = \frac{1}{2} \int_{-L/2}^{L/2} k_w (w_1 - w_2)^2 dx \tag{7}$$

where  $k_w$  is the spring constant of the elastic layer. Additive strain energy function of the translational, the rotational and the extensional springs at the ends of the beams is given as

$$U_{sup} = \frac{1}{2} \sum_{i=1}^2 \left\{ k_{ei} [u_1(x_{si}, t)]^2 + k_{ti} [w_1(x_{si}, t)]^2 + k_{ri} \left[ \frac{\partial w_1(x_{si}, t)}{\partial x} \right]^2 \right\} + \frac{1}{2} \sum_{i=3}^4 \left\{ k_{ei} [u_2(x_{si}, t)]^2 + k_{ti} [w_2(x_{si}, t)]^2 + k_{ri} \left[ \frac{\partial w_2(x_{si}, t)}{\partial x} \right]^2 \right\} \tag{8}$$

where  $k_{ei}$ ,  $k_{ti}$  and  $k_{ri}$  are the spring constants of the extensional, translational and the rotational springs, respectively.  $x_{s1}$  ( $x_{s3} = -L/2$ ,  $x_{s2} = x_{s4} = L/2$ ) denotes the location of the  $i$ th support. Potential of the concentrated moving harmonic load at any instant is given below

$$U_{ext} = - \int_{-L/2}^{L/2} Q(t) \delta(x - x_Q(t)) w_1(x, t) dx \tag{9a}$$





$$Q(t) = Q_0 \sin(\Omega t) \tag{9b}$$

$$x_Q(t) = -L/2 + v_Q t, \quad -L/2 \leq x_Q(t) \leq L/2, \quad 0 \leq t \leq L/v_Q \tag{9c}$$

where  $\delta(\cdot)$  is the Dirac delta function,  $Q_0$  is the amplitude of the moving harmonic load,  $\Omega$  is the excitation frequency of the moving harmonic load,  $x_Q(t)$  is the location of the moving load at any instant. Including the rotary inertia and the axial inertia effects, the kinetic energy of the beam,  $K_e$ , at any instant can be expressed as

$$K_e = \frac{1}{2} \sum_{i=1}^2 \left\{ \int_{-L/2}^{L/2} \left[ I_A \left( \frac{\partial u_i(x, t)}{\partial t} \right)^2 - 2I_B \left( \frac{\partial u_i(x, t)}{\partial t} \right) \left( \frac{\partial^2 w_i(x, t)}{\partial x \partial t} \right) + I_A \left( \frac{\partial w_i(x, t)}{\partial t} \right)^2 + I_D \left( \frac{\partial^2 w_i(x, t)}{\partial x \partial t} \right)^2 \right] dx \right\} \tag{10}$$

**Table 1**  
The spring constants for the different boundary conditions.

Boundary conditions	Left end spring constants	Right end spring constants
	$k_{e1} = k_{t1} = k_{r1} = 1 \times 10^{12} \text{ N/m} \approx \infty$	$k_{e2} = k_{t2} = k_{r2} = 1 \times 10^{12} \text{ N/m} \approx \infty$
	$k_{e1} = k_{t1} = k_{r1} = 1 \times 10^{12} \text{ N/m} \approx \infty$	$k_{t2} = 1 \times 10^{12} \text{ N/m} \approx \infty$ $k_{e2} = k_{r2} = 0$
	$k_{e1} = k_{t1} = 1 \times 10^{12} \text{ N/m} \approx \infty$ $k_{r1} = 0$	$k_{t2} = 1 \times 10^{12} \text{ N/m} \approx \infty$ $k_{e2} = k_{r2} = 0$
	$k_{e1} = k_{t1} = k_{r1} = 1 \times 10^{12} \text{ N/m} \approx \infty$	$k_{e2} = k_{t2} = k_{r2} = 0$

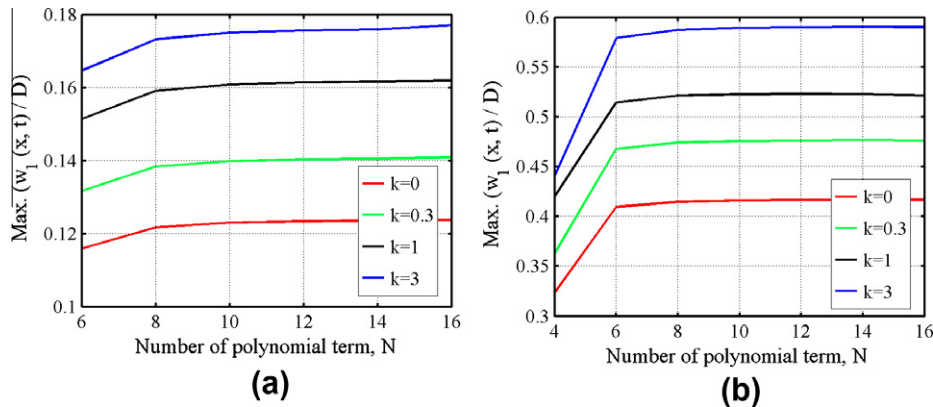


**Fig. 3.** The effect of the number of polynomial term on the non-dimensional deflections for 25 m/s,  $\kappa = 100$ , (a) CC-CC DFGBS and (b) PP-PP DFGBS.

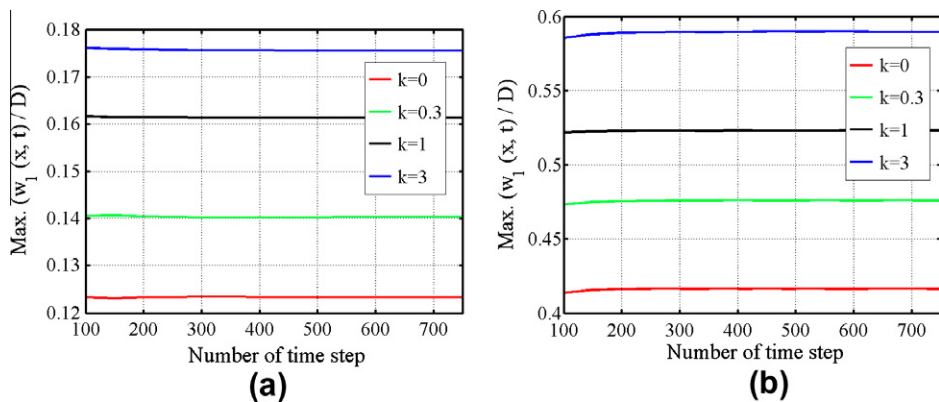


**Fig. 4.** The effect of the number of time step on the non-dimensional deflections for 25 m/s,  $\kappa = 100$ , (a) CC-CC DFGBS and (b) PP-PP DFGBS.



The inertia terms ( $I_A, I_B, I_D$ ) appearing in Eq. (10) are defined as follows:

$$(I_A, I_B, I_D) = \int_A \rho(z)(1, z, z^2) dA \quad (11)$$

where  $\rho$  is the mass density of the beam. Equations of the motion will be derived by using Lagrange's equations. It is well-known that Hamilton's principle can be expressed as Lagrange's equations when the functions of infinite dimensions can be expressed in terms

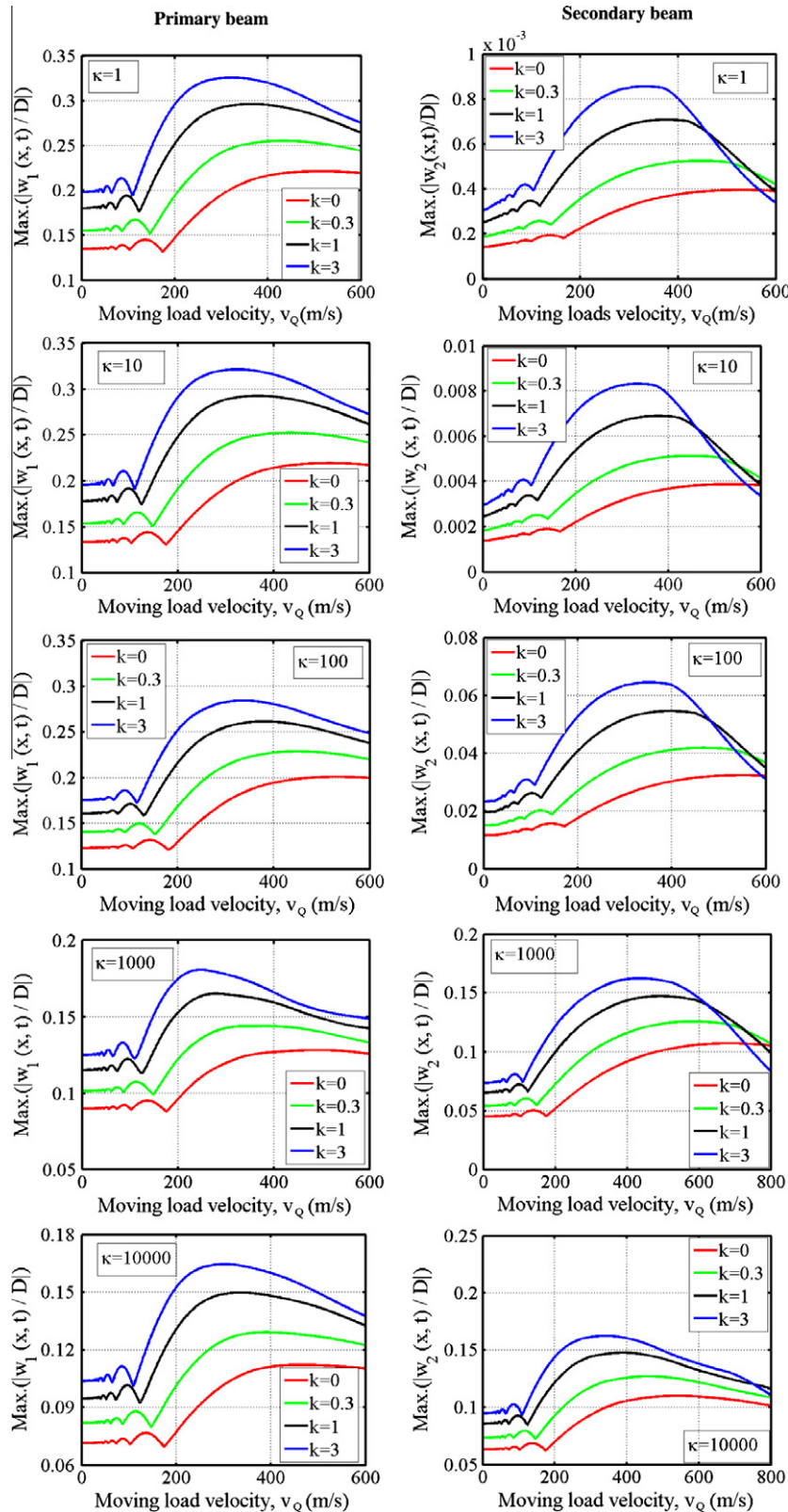


Fig. 5. Variation of the non-dimensional dynamic deflections of CC-CC DFGBS with the moving load velocity for  $\Omega = 0$  and for various values of the stiffness of the elastic layer.

of generalized coordinates  $q_n(t)$ . Therefore, the transverse and the axial displacements of DFGBS can be approximated as

$$\begin{pmatrix} w_1(x, t) \\ w_2(x, t) \\ u_1(x, t) \\ u_2(x, t) \end{pmatrix} = \sum_{n=1}^N \begin{pmatrix} A_n(t)x^{n-1} \\ B_n(t)x^{n-1} \\ C_n(t)x^{n-1} \\ D_n(t)x^{n-1} \end{pmatrix} \quad (12)$$

By introducing the following definitions;

$$q_n = A_n \quad n = 1, 2, \dots, N \quad (13a)$$

$$q_n = B_{n-N} \quad n = N + 1, \dots, 2N \quad (13b)$$

$$q_n = C_{n-2N} \quad n = 2N + 1, \dots, 3N \quad (13c)$$

$$q_n = D_{n-3N} \quad n = 3N + 1, \dots, 4N \quad (13d)$$

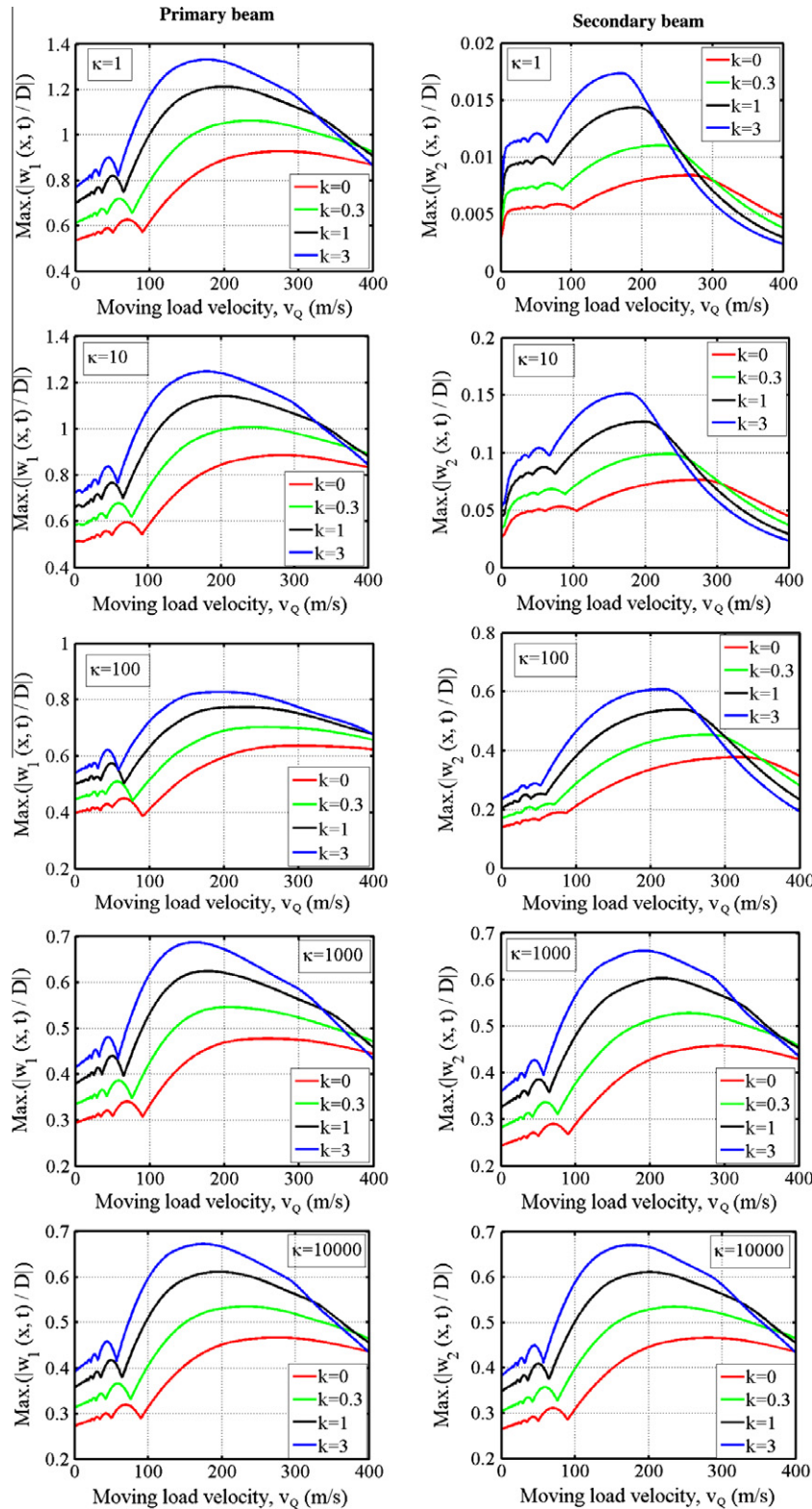


Fig. 6. Variation of the non-dimensional dynamic deflections of PP-PP DFGBS with the moving load velocity for  $\Omega = 0$  and for various values of the stiffness of the elastic layer.

and then using the Lagrange's equations given by Eq. (14)

$$\frac{d}{dt} \left( \frac{\partial K_e}{\partial \dot{q}_n} \right) + \frac{\partial U_{int}}{\partial q_n} + \frac{\partial U_{el}}{\partial q_n} + \frac{\partial U_{sup}}{\partial q_n} + \frac{\partial U_{ext}}{\partial q_n} = 0 \quad n = 1, 2, 3, \dots, 4N \quad (14)$$

yields the following system of equations of motion

$$[\mathbf{K}]\{\mathbf{q}(\mathbf{t})\} + [\mathbf{K}_s]\{\mathbf{q}(\mathbf{t})\} + [\mathbf{M}]\{\ddot{\mathbf{q}}(\mathbf{t})\} = \{\mathbf{F}(\mathbf{t})\} \quad (15)$$

where  $[\mathbf{K}]$  is the stiffness matrix, the matrix  $[\mathbf{K}_s]$  exists due to the linear springs at the end of the beams,  $[\mathbf{M}]$  is the mass matrix,

$\{\mathbf{F}(\mathbf{t})\}$  is the time-dependent generalized load vector generated by the concentrated moving harmonic load and  $\{\mathbf{q}(\mathbf{t})\} = \{\mathbf{A}(\mathbf{t}), \mathbf{B}(\mathbf{t}), \mathbf{C}(\mathbf{t}), \mathbf{D}(\mathbf{t})\}^T$ . The size of matrices  $[\mathbf{K}]$ ,  $[\mathbf{K}_s]$  and  $[\mathbf{M}]$  is  $4N \times 4N$  and the size of vector  $\{\mathbf{F}(\mathbf{t})\}$  is  $4N$ . The expanded form of Eq. (15) and the terms of  $[\mathbf{K}]$ ,  $[\mathbf{K}_s]$ ,  $[\mathbf{M}]$  and  $\{\mathbf{F}(\mathbf{t})\}$  are given in Appendix at the end of the paper. The equations of motion are solved by using the implicit time integration method of Newmark- $\beta$  and then the displacements, velocities and accelerations of the beam at the considered point and time are determined for any time  $t$  between  $0 \leq t \leq L/v_Q$ .

**Table 2**

Maximum non-dimensional dynamic deflections of CC-CC DFGBS and the corresponding critical velocities for various values of the stiffness of the elastic layer, the power-law exponent and for  $\Omega = 0$ .

Stiffness parameter, $\kappa$	Power-law exponent, $k$	Primary beam		Secondary beam	
		Max. $(w_1(x,t)/D)$	$v_{cr}$ (m/s)	Max. $(w_2(x,t)/D)$	$v_{cr}$ (m/s)
1	0	0.221	516	0.0003	530
	0.3	0.255	434	0.0005	446
	1	0.296	366	0.0007	376
	3	0.325	324	0.0008	332
10	0	0.219	518	0.003	532
	0.3	0.252	437	0.005	448
	1	0.292	368	0.007	378
	3	0.321	326	0.008	334
100	0	0.201	533	0.032	551
	0.3	0.228	447	0.041	467
	1	0.261	379	0.054	396
	3	0.284	336	0.064	352
1000	0	0.128	492	0.107	687
	0.3	0.143	375	0.125	582
	1	0.165	280	0.147	493
	3	0.180	248	0.162	435
10,000	0	0.112	466	0.110	538
	0.3	0.129	389	0.127	462
	1	0.149	337	0.147	390
	3	0.164	300	0.162	341

**Table 3**

Maximum non-dimensional dynamic deflections of CP-CP DFGBS and the corresponding critical velocities for various values of the stiffness of the elastic layer, the power-law exponent and for  $\Omega = 0$ .

Stiffness parameter, $\kappa$	Power-law exponent, $k$	Primary beam		Secondary beam	
		Max. $(w_1(x,t)/D)$	$v_{cr}$ (m/s)	Max. $(w_2(x,t)/D)$	$v_{cr}$ (m/s)
1	0	0.393	459	0.0014	377
	0.3	0.453	387	0.0019	318
	1	0.526	326	0.0026	268
	3	0.578	288	0.0032	237
10	0	0.385	463	0.014	381
	0.3	0.443	390	0.018	321
	1	0.512	329	0.025	271
	3	0.562	290	0.030	240
100	0	0.325	482	0.100	414
	0.3	0.366	406	0.126	353
	1	0.413	349	0.160	301
	3	0.446	310	0.186	268
1000	0	0.208	337	0.199	567
	0.3	0.238	297	0.227	490
	1	0.274	266	0.260	414
	3	0.300	251	0.284	352
10,000	0	0.197	455	0.197	460
	0.3	0.227	387	0.227	385
	1	0.263	321	0.264	322
	3	0.290	285	0.290	288

**Table 4**

Maximum non-dimensional dynamic deflections of PP-PP DFGBS and the corresponding critical velocities for various values of the stiffness of the elastic layer, the power-law exponent and for  $\Omega = 0$ .

Stiffness parameter, $\kappa$	Power-law exponent, $k$	Primary beam		Secondary beam	
		Max. $(w_1(x,t)/D)$	$v_{cr}$ (m/s)	Max. $(w_2(x,t)/D)$	$v_{cr}$ (m/s)
1	0	0.927	279	0.008	269
	0.3	1.069	235	0.011	228
	1	1.241	198	0.015	192
	3	1.362	175	0.018	170
10	0	0.885	280	0.076	277
	0.3	1.014	238	0.100	234
	1	1.167	202	0.132	198
	3	1.276	179	0.158	176
100	0	0.636	300	0.377	320
	0.3	0.706	254	0.457	273
	1	0.786	216	0.556	234
	3	0.841	183	0.627	215
1000	0	0.477	258	0.458	294
	0.3	0.549	205	0.531	251
	1	0.639	176	0.617	215
	3	0.704	159	0.677	189
10,000	0	0.467	274	0.465	281
	0.3	0.538	233	0.537	235
	1	0.625	194	0.625	199
	3	0.688	173	0.687	174

**Table 5**

Maximum non-dimensional dynamic deflections of CF-CF DFGBS and the corresponding critical velocities for various values of the stiffness of the elastic layer, the power-law exponent and for  $\Omega = 0$ .

Stiffness parameter, $\kappa$	Power-law exponent, $k$	Primary beam		Secondary beam	
		Max. $(w_1(x,t)/D)$	$v_{cr}$ (m/s)	Max. $(w_2(x,t)/D)$	$v_{cr}$ (m/s)
1	0	2.892	95	0.148	75
	0.3	3.316	80	0.194	62
	1	3.819	66	0.258	54
	3	4.175	61	0.310	46
10	0	2.217	98	0.832	85
	0.3	2.488	84	1.026	72
	1	2.790	68	1.266	62
	3	3.015	61	1.466	56
100	0	1.596	88	1.421	88
	0.3	1.825	75	1.659	75
	1	2.100	62	1.951	62
	3	2.295	55	2.156	55
1000	0	1.503	89	1.513	89
	0.3	1.734	75	1.745	75
	1	2.013	63	2.026	63
	3	2.215	55	2.228	55
10,000	0	1.508	89	1.509	89
	0.3	1.739	75	1.739	75
	1	2.019	63	2.020	63
	3	2.221	56	2.222	56

### 3. Numerical results

In this section, the effects of the material composition, velocity of the moving harmonic load, forcing frequency, the stiffness of the elastic layer between the FG beams and the boundary conditions on the dynamic responses of DFGBS are discussed in detail. The physical system considered in this study is an elastically connected double-beam system, composed of two parallel FG beams with uniformly distributed-connecting springs among them. The FG beams of DFGBS are composed of Steel (SUS304;  $E = 210$  GPa,  $\rho = 7800$  kg/m<sup>3</sup>) and Alumina (Al<sub>2</sub>O<sub>3</sub>; Al;  $E = 390$  GPa,  $\rho = 3960$  kg/m<sup>3</sup>) and its properties change through the thickness of the beam according to the power-law. The bottom surfaces of the FG beams are pure steel, whereas the top surfaces of the beams are pure alumina. The dimensions of the FG beams are as follows:  $b = 0.5$  m,  $h = 1$  m,  $L = 20$  m. Six models with different boundary conditions are considered. These are:

- The primary beam clamped–clamped, the secondary beam clamped–clamped (CC–CC).
- The primary beam clamped–pinned, the secondary beam clamped–pinned (CP–CP).
- The primary beam pinned–pinned, the secondary beam pinned–pinned (PP–PP).
- The primary beam clamped–free, the secondary beam clamped–free (CF–CF).
- The primary beam pinned–pinned, the secondary beam clamped–clamped (PP–CC).
- The primary beam pinned–pinned, the secondary beam clamped–free (PP–CF).

In the above notation, the first letters denote the primary beam; the second letters denote the secondary beam. The point constraints of the supports are modeled as linear springs of very large stiffness. These linear springs of sufficiently large stiffness will ensure that the points where the springs attached will remain stationary during the transverse deformation of the beam. For example, the spring constants are taken as  $k_{ei} = k_{ti} = k_{ri} = 1 \times 10^{12}$  N/m

for the clamped end, and  $k_{ei} = k_{ti} = 1 \times 10^{12}$  N/m,  $k_{ri} = 0$  for the pinned end (see Table 1 for the other boundary conditions). In the numerical analysis, in order to ensure the homogeneity among the results of the six models with different end conditions, the dynamic deflections of the six models are normalized by the same static deflection  $D = Q_0 L^3 / 48 E_{steel} I$  of the fully steel beam under a point load  $Q_0$  at the mid-span of the beam. Therefore, the normalized dynamic deflections do not depend on the magnitude of the moving load  $Q(t)$ . The effect of the elastic layer stiffness is considered by the dimensionless parameter ( $\kappa$ ) as follows:

$$\kappa = \frac{k_w L^4}{E_{steel} I} \tag{16}$$

Also, the dimensionless time  $t^*$  is defined by

$$t^* = \frac{x_Q}{L} = \frac{-L/2}{L} + \frac{v_Q t}{L} = -\frac{1}{2} + \frac{v_Q t}{L} \tag{17}$$

Therefore, when  $t^* = -0.5$  the moving harmonic load is at the left edge of the beam, i.e.,  $x_Q = -L/2$ , and when  $t^* = 0.5$  the load is at the right edge of the beam, i.e.,  $x_Q = L/2$ .

Figs. 3 and 4 show the effect of the number of the polynomial term and the number of time step in Newmark integration method on the maximum non-dimensional dynamic deflections of DFGBS with CC–CC and PP–PP boundary conditions. These figures are given for CC–CC and PP–PP boundary conditions with  $\kappa = 100$  for the sake of the brevity since similar results are obtained for the other boundary conditions and the other parameter. It is seen from Figs. 3 and 4 that the dynamic deflections are saturated when twelve terms are taken, and the numerical accuracy of the responses improved only slightly when the number of time step is taken to be more than 100. From the analysis conducted, setting the number of the modes to 12 and the number of time step to 500 is very satisfactory for the desired numerical precision in the subsequent numerical calculations.

Figs. 5 and 6 present the maximum non-dimensional dynamic deflections of the primary and the secondary beams of DFGBSs as a function of the moving load velocity for the two different boundary conditions. In these figures, the maximum dimensionless dy-

**Table 6**  
Maximum non-dimensional dynamic deflections of PP–CC DFGBS and the corresponding critical velocities for various values of the stiffness of the elastic layer, the power-law exponent and for  $\Omega = 0$ .

Stiffness parameter, $\kappa$	Power-law exponent, $k$	Primary beam		Secondary beam	
		Max. ( $w_1(x,t)/D$ )	$v_{cr}$ (m/s)	Max. ( $w_2(x,t)/D$ )	$v_{cr}$ (m/s)
1	0	0.927	280	0.0013	372
	0.3	1.069	235	0.0017	313
	1	1.241	198	0.0024	263
	3	1.365	175	0.0029	233
10	0	0.885	283	0.012	381
	0.3	1.013	239	0.016	319
	1	1.166	202	0.022	271
	3	1.274	179	0.027	240
100	0	0.617	337	0.088	440
	0.3	0.681	293	0.112	376
	1	0.752	246	0.142	315
	3	0.800	215	0.164	286
1000	0	0.237	395	0.172	600
	0.3	0.262	339	0.195	508
	1	0.292	290	0.223	424
	3	0.313	260	0.242	369
10,000	0	0.152	443	0.152	514
	0.3	0.173	384	0.173	431
	1	0.199	329	0.199	354
	3	0.217	291	0.218	314

**Table 7**  
Maximum non-dimensional dynamic deflections of PP–CF DFGBS and the corresponding critical velocities for various values of the stiffness of the elastic layer, the power-law exponent and for  $\Omega = 0$ .

Stiffness parameter, $\kappa$	Power-law exponent, $k$	Primary beam		Secondary beam	
		Max. ( $w_1(x,t)/D$ )	$v_{cr}$ (m/s)	Max. ( $w_2(x,t)/D$ )	$v_{cr}$ (m/s)
1	0	0.927	277	0.013	110
	0.3	1.069	235	0.018	94
	1	1.241	198	0.024	80
	3	1.365	175	0.029	71
10	0	0.885	283	0.101	139
	0.3	1.013	239	0.128	120
	1	1.166	202	0.165	104
	3	1.275	179	0.193	94
100	0	0.624	322	0.227	231
	0.3	0.689	283	0.324	201
	1	0.763	243	0.380	177
	3	0.813	214	0.420	159
1000	0	0.325	275	0.266	325
	0.3	0.364	237	0.308	284
	1	0.410	205	0.357	250
	3	0.443	184	0.392	229
10,000	0	0.242	413	0.241	435
	0.3	0.276	353	0.276	366
	1	0.318	302	0.318	308
	3	0.348	268	0.348	265



dynamic deflections at the center of the beams are plotted versus the corresponding velocities with 1 m/s increments for various values of the power-law exponent ( $k = 0, 0.3, 1, 3$ ) and the stiffness of the elastic layer ( $\kappa = 1, 10, 100, 1000, 10,000$ ). In order to avoid the inclusion of too many figures to this paper, only some curves for CC–CC and PP–PP DFGBS will be shown. According to these figures, it is discerned that the non-dimensional dynamic deflections generally improve until a certain value of the moving load velocity, and after this value, increase in the velocity leads to a decrease in the non-dimensional dynamic deflections. This velocity, which makes the vibration amplitude reach its maximum value, is called the critical velocity. It is seen from the figures that as the steel constituent increases in DFGBS, i.e., the power-law exponent ( $k$ ) increases, the non-dimensional deflections of the primary and the secondary beams also increase. The increasing in the power-law exponent is seen to significantly decrease the structural stiffness hence the bending rigidity. It should be noted that when the power-law exponent ( $k$ ) approaches to zero, the material properties of the two FG beam approach to those of pure alumina and

when the power-law exponent ( $k$ ) approaches to infinity, the material properties of the two FG beam approach to those of pure steel. From the depicted results in Figs. 5 and 6, it is observed that as the stiffness of the elastic layer parameter ( $\kappa$ ) increases the deflections of the primary beam decrease while the deflections of the secondary beam increase. When the stiffness of the elastic layer parameter ( $\kappa$ ) takes very small value (i.e.,  $\kappa = 1$ ), the deflections of the secondary beams are also very small. This is due to the weak elastic coupling between the primary and the secondary beams. Further investigation shows that the non-dimensional deflections of the two beams become equal to each other for the very large value of the stiffness of the elastic layer parameter (i.e.,  $\kappa = 10,000$ ). The situation for the very large values of  $\kappa$  can be defined as rigid coupling between the two beams. The deflections of the two beams are equal to each other since the two beams behave like a single beam in the case of the rigid coupling. It should be noted at this stage that Khalili et al. [43] and Yan et al. [46] compared their results with the results of the author's previous study [42], which examines the dynamic behavior of a single FG beam

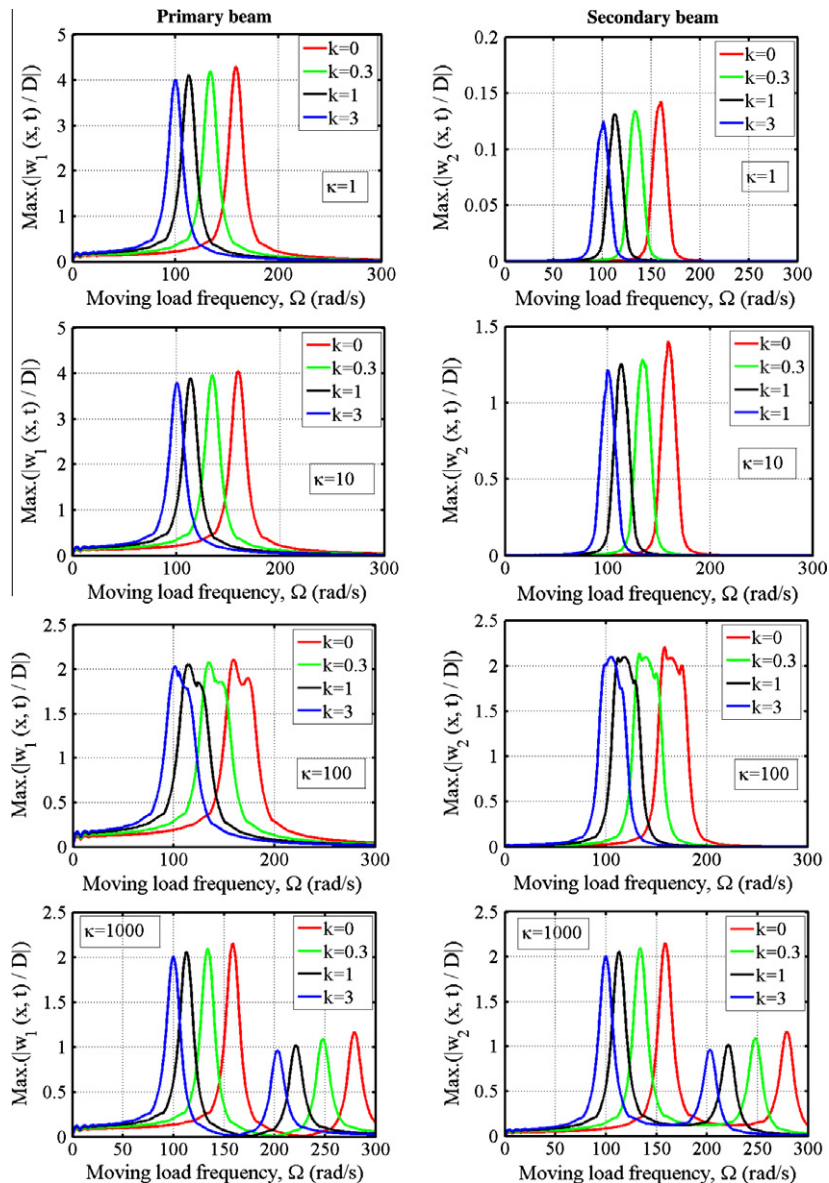


Fig. 7. Variation of the non-dimensional dynamic deflections of CC–CC DFGBS with the moving load frequency for  $v = 25$  m/s and for various values of the stiffness of the elastic layer.

under a moving harmonic load. The comparisons show that the maximum non-dimensional deflections and the corresponding critical velocities of the companion paper [42] are in good agreement with the results of Refs. [43,46].

In Tables 2–7, the maximum magnitudes of the maximum non-dimensional dynamic deflections of the primary and the secondary beams and the corresponding critical velocities (the velocities at which the maximum magnitudes of the maximum deflections to be occurred) are provided for the six different boundary conditions, different material properties and stiffness of the elastic layer. As expected, DFGBS with CC–CC boundary conditions, which is the most rigid model, gives the lowest deflections; on the other hand the largest deflections are found for DFGBS with CF–CF boundary conditions, which is the least rigid model. It is clearly seen that for a fixed value of the stiffness of the elastic layer parameter ( $\kappa$ ), the critical velocities of both beams of the all models decrease when the power-law exponent increases. The critical velocity is very sensitive to the power-law exponent ( $k$ ). Hence, the critical

velocity can also be controlled by choosing suitable values of the power-law exponent ( $k$ ). Another important result from these tables is that the highest critical velocities are found for CC–CC DFGBS, which is the most rigid model whereas the lowest critical velocities are obtained for the CF–CF DFGBS, which is the least rigid one. Based on the above two results on the critical velocity, it can be said that the critical velocity decreases as the stiffness of the system increases. However, a similar conclusion related to critical velocity are not deduced from the data presented in Tables 2–7 even if the stiffness of the elastic layer parameter ( $\kappa$ ) increases the stiffness of the system. Furthermore, it is interestingly found that the rate of increase in the critical velocity due to an increase in the power-law exponent ( $k$ ) ranges from 32% to 38% for the all boundary conditions regardless of the stiffness of the elastic layer parameter ( $\kappa$ ). It is obvious from the tables that the critical velocities are generally very high for such beams made of steel and alumina and it is very difficult to reach these velocities in practical applications. For instance, it is found  $v = 516 \text{ m/s} = 1857.6 \text{ km/h}$

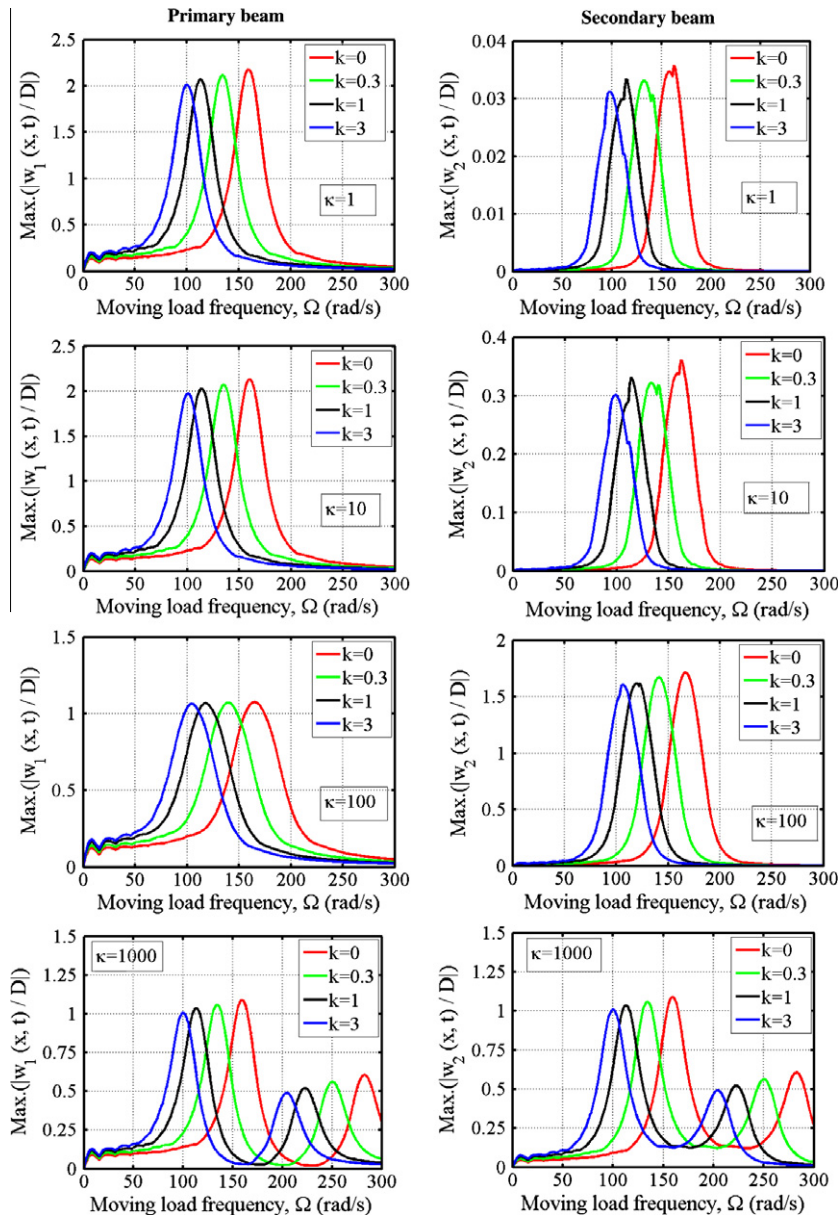


Fig. 8. Variation of the non-dimensional dynamic deflections of CC–CC DFGBS with the moving load frequency for  $v = 50 \text{ m/s}$  and for various values of the stiffness of the elastic layer.

and  $v = 279 \text{ m/s} = 1044.2 \text{ km/h}$  for CC–CC and PP–PP DFGBS with  $k = 0, \kappa = 1$ , respectively. On the other hand, for a single concrete beam with the same geometrical properties, critical velocities are found  $v = 147 \text{ m/s} = 529.2 \text{ km/h}$  and  $v = 79 \text{ m/s} = 284.4 \text{ km/h}$  for CC–CC and PP–PP DFGBS, respectively. Therefore, concrete systems are more vulnerable to damage under the service loads. For this reason, construction of these systems from FGMs can be advantageous for future applications. It can be seen from the tables that for the all models with different material properties, the maximum non-dimensional deflections of the two beams are the half of the maximum normalized deflection of a single beam in the rigid coupling case. This is due to the fact that in the case of the rigid coupling, the two FG beams oscillate like a single beam with double stiffness ( $2D_{xx}, 2B_{xx}, 2A_{xx}$ ). Also, it is worth pointing out that except for CC–CC and PP–CC DFGBS, the critical velocity of the primary and secondary beams is almost the same for the considered values of  $\kappa$  parameter in the rigid coupling situation. However, the critical velocity of the primary and secondary beams become almost the same for CC–CC and PP–CC DFGBS when  $\kappa \geq 30000$ .

In order to assess the influence of the excitation frequency of the moving harmonic load on dynamic behavior of DFGBSs, the variation of the maximum absolute values of the non-dimensional dynamic deflections of the primary and the secondary beams with the excitation frequency are given in Figs. 7–10 for the selected values of the moving load velocity ( $v = 25, 50 \text{ m/s}$ ) and various values of the power-law exponent. In these figures, the maximum absolute values of the dynamic deflections are considered since the maximum displacements may be occurred in the negative region depending on the excitation frequency. However, in the case of the moving load with constant magnitude, the maximum displacement is always occurred in the positive region. It is shown that very large displacements (peak values) are obtained at some frequency values. This frequency value, which makes the displacements very large, is the fundamental frequency of DFGBS. It is clear that fundamental frequency of DFGBS decreases as the power-law exponent increases. The reason for this behavior is considered to be as follows: As stated earlier, DFGBSs become softer with an increase in the power-law exponent ( $k$ ), and it is known that free

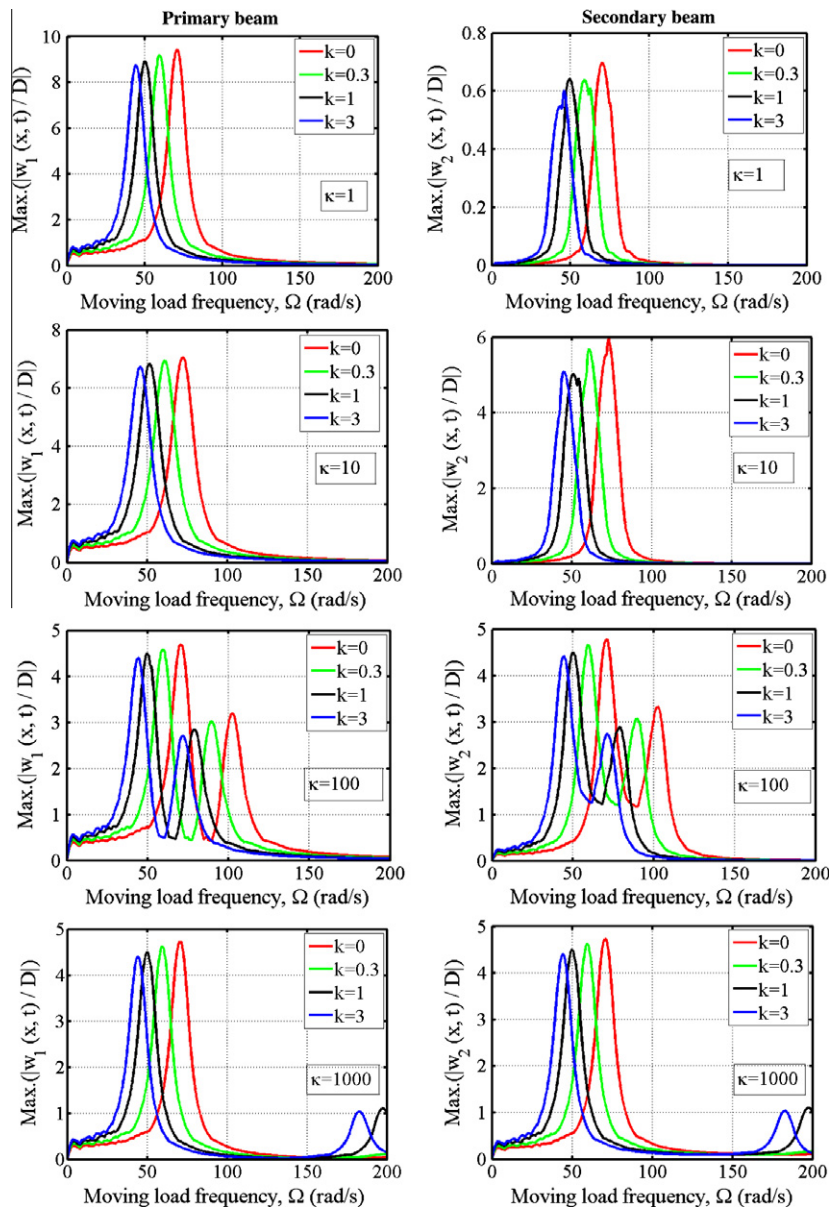


Fig. 9. Variation of the non-dimensional dynamic deflections of PP–PP DFGBS with the moving load frequency for  $v = 25 \text{ m/s}$  and for various values of the stiffness of the elastic layer.



vibration frequencies decrease when structural rigidity decreases. Related to the above interpretation, it seen from these figure that fundamental frequency of CC–CC DFGBS is higher than that of PP–PP DFGBS. The most important conclusion from these figures

is due to the fact that two fundamental frequencies are obtained at some specific values of the elastic layer parameter (i.e., CC–CC DFGBS with  $\kappa = 1000$  and PP–PP DFGBS with  $\kappa = 100, 1000$ ) for the considered values of the excitation frequency. Also, the lowest

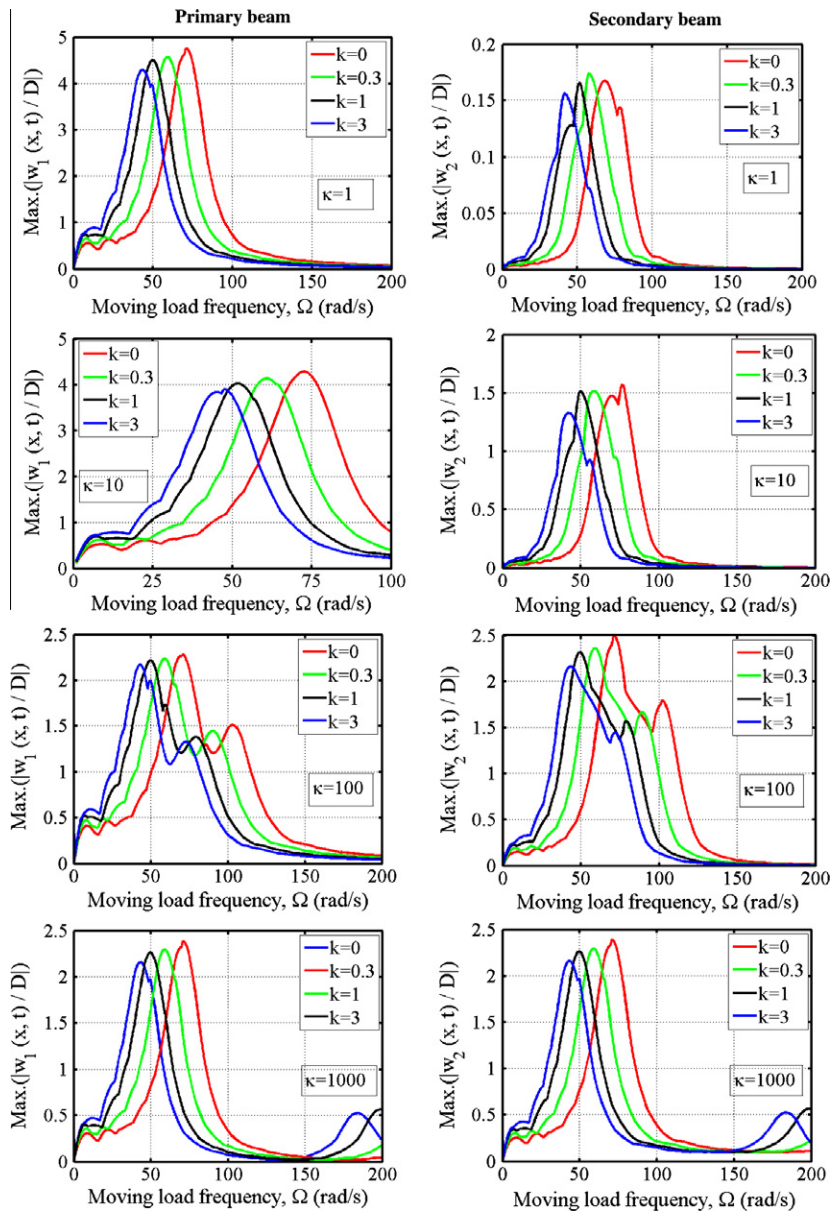


Fig. 10. Variation of the non-dimensional dynamic deflections of PP–PP DFGBS with the moving load frequency for  $v = 50$  m/s and for various values of the stiffness of the elastic layer.

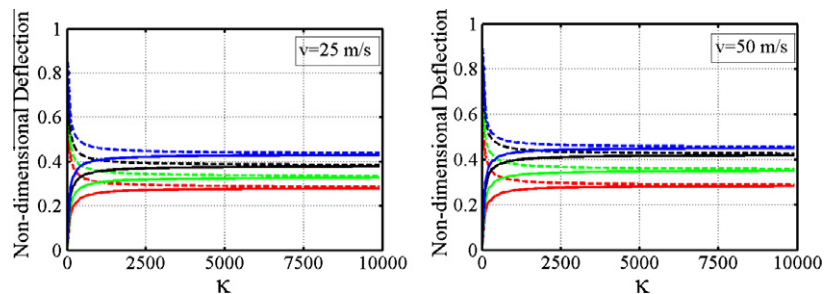


Fig. 11. Variation of the non-dimensional dynamic deflections of PP–PP DFGBS of the primary beam with the stiffness of the elastic layer for  $\Omega = 0$ , (—)  $k = 0$ , (—)  $k = 0.3$ , (---)  $k = 1$ , (—)  $k = 3$ , solid lines: Primary beam, dashed lines: Secondary beam.



fundamental frequency of DFGBS is not dependent on the stiffness of the elastic layer parameter ( $\kappa$ ) and it is the same as for a single beam (see the all first peaks). It should be noted at this stage that a double-beam system has two infinite sequences of the natural frequencies. One of them is called synchronous natural frequencies, which are independent of the elastic layer between the beams and are the same as for a single beam. In synchronous vibration, the elastic layer between the beams is not deformed in the transverse direction. The other set of natural frequencies is called asynchronous natural frequencies, which are identical as for a single beam vibrating on an elastic foundation of stiffness modulus  $2k_w$  [47]. In this context, it can be summarized that a double-beam system has two fundamental frequencies, which are called synchronous ( $\omega_{11}$ ) and asynchronous fundamental frequency ( $\omega_{21}$ ). For instance, when the power-law exponent is taken as ( $k = 1$ ) for PP-PP DFGBS (see Fig. 9), the first peak is seen at  $\Omega = \omega_{11} = 50.047$  rad/s for the all  $\kappa$  values. This frequency is the synchronous fundamental frequency, which is independent of the elastic layer

parameter. On the other hand, the second peak is obtained for  $\Omega = \omega_{21} = 78.84$  rad/s, which causes also relatively large displacement. This frequency, which depends on the elastic layer parameter, is called asynchronous fundamental frequency. Moreover, when the moving load velocity are increased from  $v = 25$  m/s to  $v = 50$  m/s, the magnitude of the deflection peaks decrease, and moreover the second deflection peak of PP-PP DFGBS are nearly disappeared (see Fig. 10).

Fig. 11 shows the effect of the stiffness of the elastic layer parameter ( $\kappa$ ) on the maximum non-dimensional deflections for the different values of the power-law exponent and two different moving load velocities ( $v = 25, 50$  m/s). These figures reveal that the primary and the secondary beams behave reversely as the parameter  $\kappa$  increases. For very large value of  $\kappa$ , the two beam vibrate together as a unit and the deflection values of the two beams approach to each other, as seen from the figures. As stated before, this is due to the fact the coupling between the two beams increases because of the increase in the parameter  $\kappa$ .

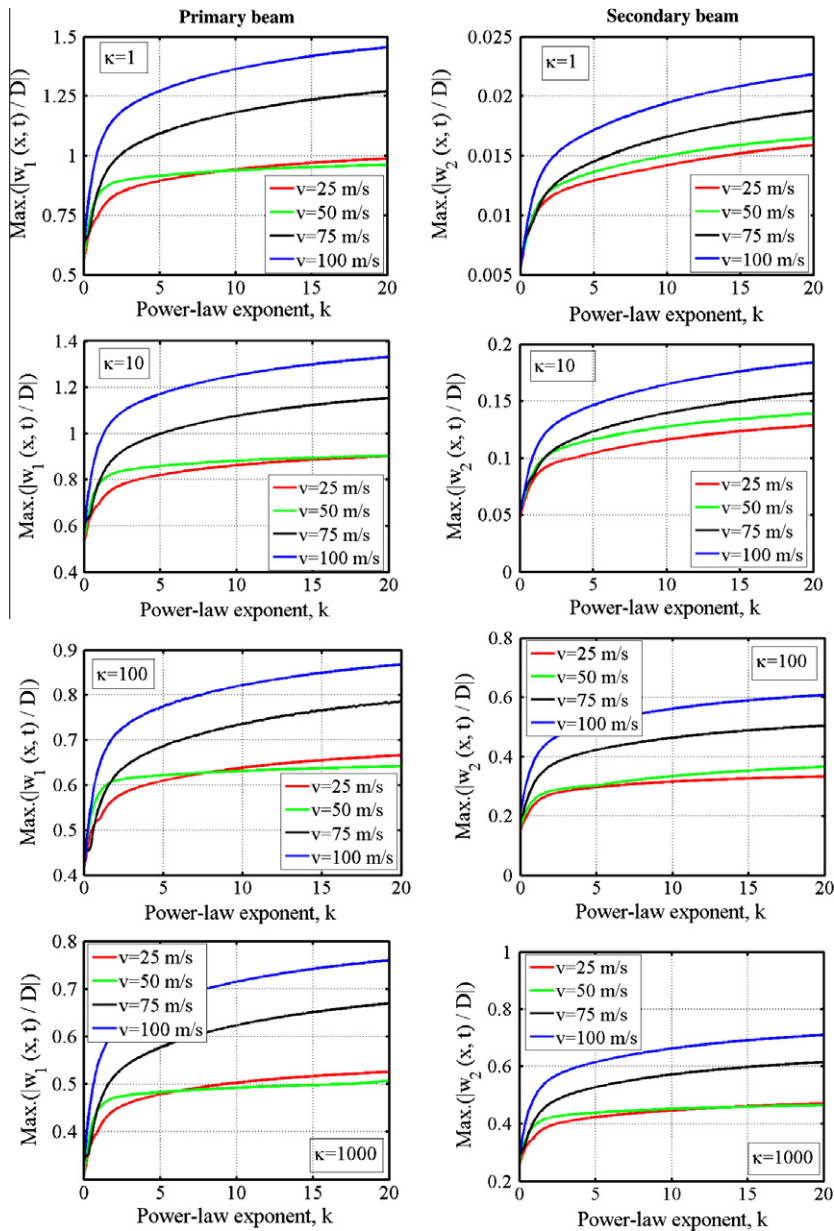


Fig. 12. Variation of the non-dimensional dynamic deflections of PP-PP DFGBS with the power-law exponent for  $\Omega = 0$  for various values of the stiffness of the elastic layer.

Figs. 12 and 13 plot the maximum non-dimensional deflections of PP-PP DFGBS with the power-law exponent ( $k$ ) for  $\kappa = 1, 10, 100, 1000$  and four different moving load velocities. For the sake of brevity, the results provided in this section are given for only PP-PP DFGBS. The most important observation from these figures that a prominent increase in the deflections occurs when the power-law exponent changes between 0 and 5, but after passing 5 all of the curves become flatter. In the case of the moving load with constant magnitude shown in Fig. 12, the dynamic deflections are steadily increase with the power-law exponent ( $k$ ) for the all considered velocity values. However, when the moving load is harmonic as given in Fig. 13 (i.e.,  $\Omega = 25$  rad/s), the dynamic deflections decrease for  $v = 25$  m/s even if the power-law exponent increases in the interval  $2 \leq k \leq 3.4$ . For instance, it is interesting to note that when  $\Omega = 25$  rad/s, the maximum absolute value of  $w_1/D$  is found as  $Max. (|w_1/D|) = |-1.0399| = 1.0399$  for  $k = 2.1$  in the negative region. On the other hand, it is obtained as  $Max. (|w_1/D|) = |1.0286| = 1.0286$  for  $k = 3.3$  in the positive region. This may be due to the interaction among the moving load velocity, the excitation frequency and the fundamental frequency which is affected by the variation of  $k$  (namely, dynamic characteristic of the problem). It is therefore concluded that the power-law exponent has a great influence on the dynamic behavior of DFGBS and the deflections of DFGBS can be controlled by choosing proper values of  $k$ .

Figs. 14 and 15 show the time histories of the primary and the secondary beams at the midspan for various values of the moving load velocity ( $v = 25, 50, 75, 100$  m/s). The power-law exponent is kept constant as  $k = 1$  and two different forcing frequencies ( $\Omega = 0, 50$  rad/s) are considered. Inspection of the figures reveals that the deflection of the secondary beam is very small for the case of the weak elastic coupling (i.e.,  $\kappa = 1$ ) and as discussed before, the time history curves of the two beams begin to close up while the power-law exponent increases. The fundamental frequency of the DFGBS

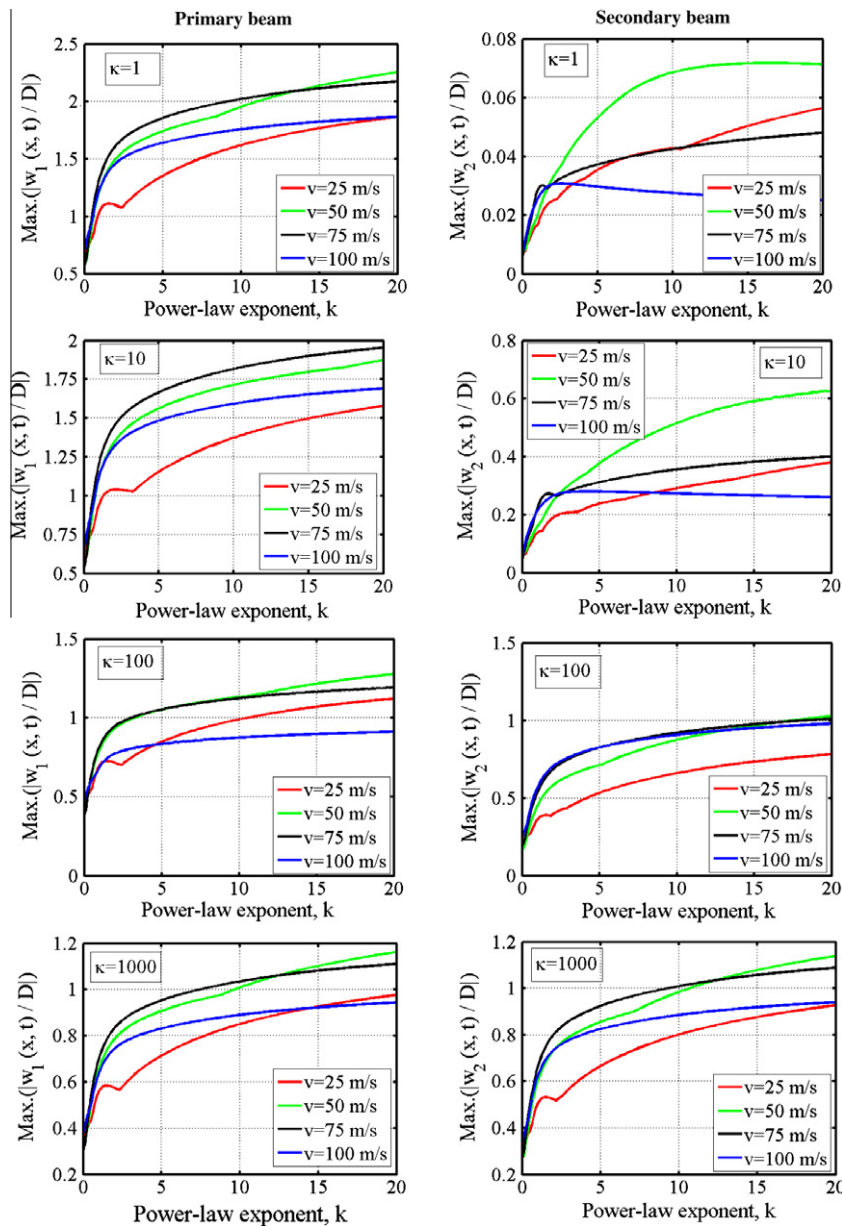


Fig. 13. Variation of the non-dimensional dynamic deflections of PP-PP DFGBS with the power-law exponent for  $\Omega = 25$  rad/s for various values of the stiffness of the elastic layer.

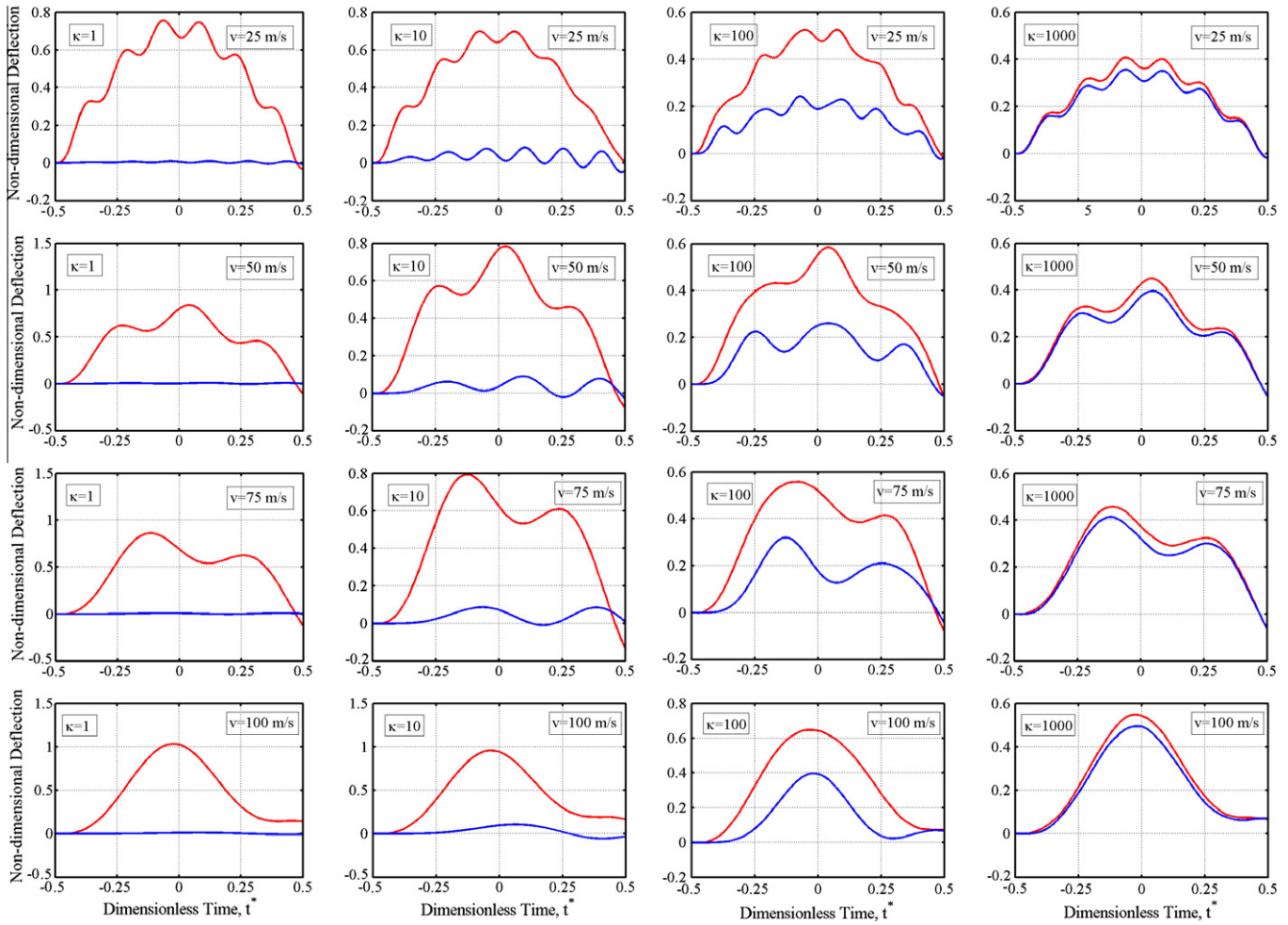


Fig. 14. Time history of the midspan deflections of PP-PP DFGBS for various values of the moving load velocity and  $k = 1, \Omega = 0$ , (—) primary beam, (—) secondary beam.

is found as 50.047 rad/s and it is independent of the elastic layer stiffness. When the forcing frequency is taken close to the fundamental frequency of the system (resonance case), very large displacements are obtained (see Fig. 15). In contrast to the moving constant load, it is seen that the dynamic deflections are continuously decreased in the resonance case as the load velocity increases. Although there is a little difference between the deflection curves for  $\kappa = 1000$  in the case of the moving constant load (see the last column of Fig. 14), the counterpart curves coincide with each other in the resonance case for  $\kappa = 1000$  (see the last column of Fig. 15).

**4. Conclusions**

In this article, a numerical method is presented to investigate the dynamic behavior of DFGBS subjected to a moving harmonic load at a constant speed based on Euler–Bernoulli beam theory. The two parallel functionally graded (FG) beams are connected with each other continuously by elastic springs. Six elastically connected double-functionally graded beam systems (DFGBS) having different boundary conditions, which are combination of pinned, clamped and free end supports, are considered. The point constraints of the supports are modeled as linear springs of very large stiffness. These linear springs of sufficiently large stiffness will ensure that the points where the springs attached will remain stationary during the transverse deformation of the beam. Material properties of the beams vary continuously in the thickness direc-

tion according to the power-law form. The equations of motion are derived with the aid of Lagrange’s equations. The unknown functions denoting the transverse deflections of DFGBS are expressed in polynomial form. Newmark method is employed to find the dynamic responses of DFGBS subjected to a concentrated moving harmonic load. The influences of the different material distribution, velocity of the moving harmonic load, forcing frequency, the rigidity of the elastic layer between the FG beams and the boundary conditions on the dynamic responses are discussed. From the results analyzed above, the most important observations are summarized as follows:

- The deflections of the primary beam decrease and those of the secondary beam increase as the elastic layer stiffness parameter increases, and they become to equal to each other in the case of rigid coupling.
- The critical velocity is very sensitive to the power-law exponent. The critical velocities of both beams of the all models decrease when the power-law exponent increases for a fixed value of the stiffness of the elastic layer parameter. Therefore, the critical velocity can also be controlled by choosing the suitable values of the power-law exponent.
- The highest critical velocities are found for CC-CC DFGBS whereas the lowest critical velocities are obtained for CF-CF DFGBS. From the numerical results, it can be concluded that the critical velocity decreases as the stiffness of the system increases.



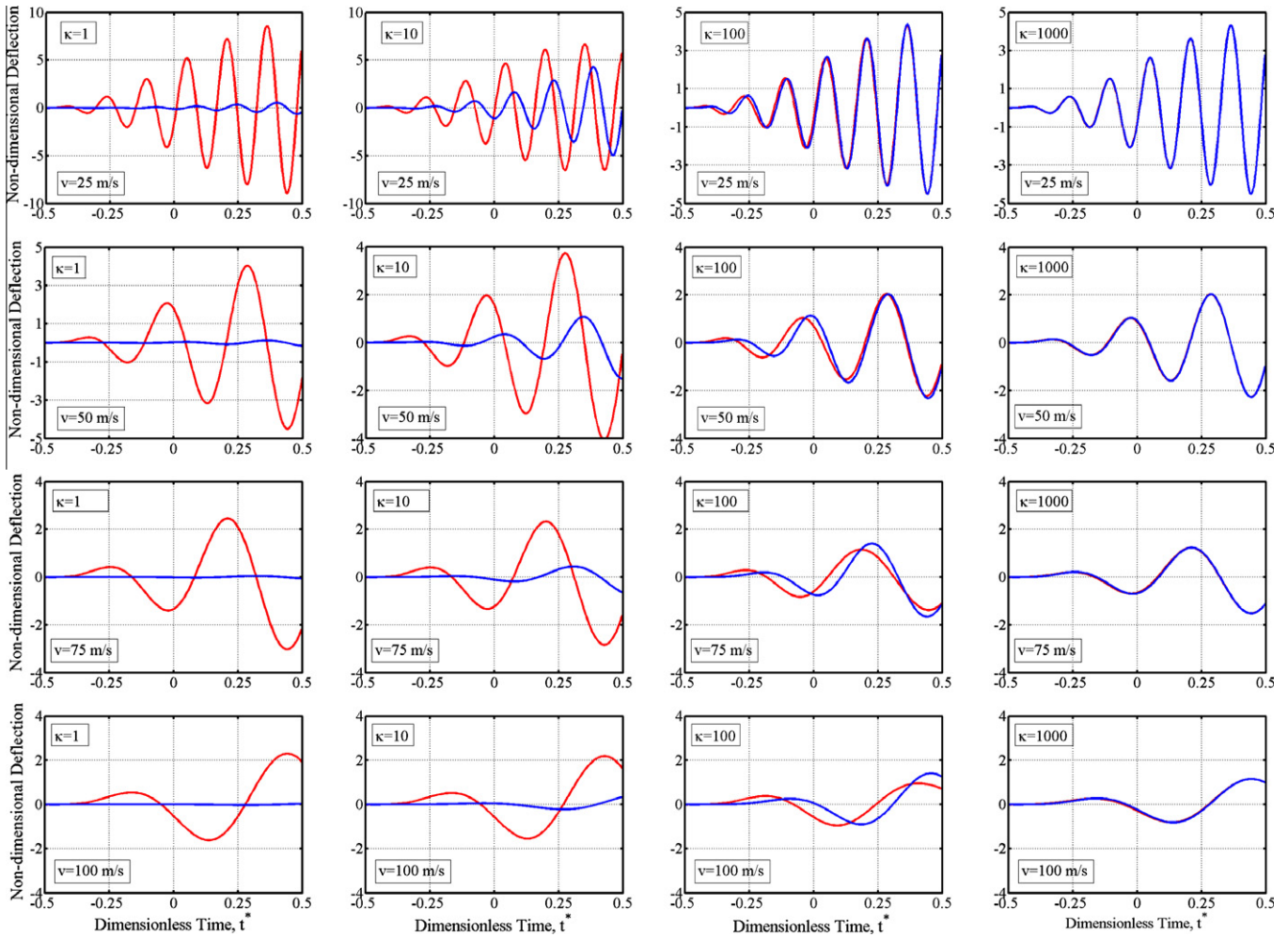


Fig. 15. Time history of the midspan deflections of PP-PP DFGBS for various values of the moving load velocity and  $k = 1$ ,  $\Omega = 50$  rad/s, (—) primary beam, (—) secondary beam.

- It is interesting to note that regardless of the stiffness of the elastic layer parameter, the rate of increase in the critical velocity due to an increase in the power-law exponent changes from %32 to %38 for the all models.
- The critical velocities of such beams made of steel and alumina are much higher than those of similar concrete beams, and it is very difficult to reach these velocities in practical applications. This may be advantageous for future applications.
- The power-law exponent has a great influence on the dynamic behavior of DFGBS and the deflections of DFGBS can be controlled by choosing proper values of  $k$ .
- DFGBS has two fundamental frequencies, which are called synchronous and asynchronous fundamental frequency. The synchronous fundamental frequency is independent of the elastic layer between the beams whereas asynchronous fundamental frequency depends on the elastic layer.
- In contrast to the moving constant load, the dynamic deflections are continuously decreased in the resonance case as the load velocity increases.
- The present formulation is very useful to analyze double or multiple-beam system with arbitrary forcing function and arbitrary boundary conditions including elastic support, multiple-beam system whose elements are made of different material composition, those with variable cross-section, etc.
- New results are presented for dynamics of DFGBSs under moving loads which are of interest to the scientific and engineering community in the area of FGM structures.

### Appendix A

The equations of motion (15) can be written in an explicit form as follows:

$$\begin{bmatrix} [K_1] & [K_2] & [K_3] & [0] \\ [K_4] & [K_5] & [0] & [K_6] \\ [K_7] & [0] & [K_8] & [0] \\ [0] & [K_9] & [0] & [K_{10}] \end{bmatrix} \begin{Bmatrix} \mathbf{A}(t) \\ \mathbf{B}(t) \\ \mathbf{C}(t) \\ \mathbf{D}(t) \end{Bmatrix} + \begin{bmatrix} [K_{S1}] & [0] & [0] & [0] \\ [0] & [K_{S2}] & [0] & [0] \\ [0] & [0] & [K_{S3}] & [0] \\ [0] & [0] & [0] & [K_{S4}] \end{bmatrix} \begin{Bmatrix} \mathbf{A}(t) \\ \mathbf{B}(t) \\ \mathbf{C}(t) \\ \mathbf{D}(t) \end{Bmatrix} + \begin{bmatrix} [M_{M1}] & [0] & [M_2] & [0] \\ [0] & [M_3] & [0] & [M_4] \\ [M_5] & [0] & [M_6] & [0] \\ [0] & [M_7] & [0] & [M_8] \end{bmatrix} \begin{Bmatrix} \dot{\mathbf{A}}(t) \\ \dot{\mathbf{B}}(t) \\ \dot{\mathbf{C}}(t) \\ \dot{\mathbf{D}}(t) \end{Bmatrix} = \begin{Bmatrix} \mathbf{f}(t) \\ \mathbf{0} \\ \mathbf{0} \\ \mathbf{0} \end{Bmatrix} \quad (A1)$$

where  $[K_1]$ – $[K_{10}]$  are the stiffness matrices,  $[K_{S1}]$ – $[K_{S4}]$  are the matrices exist due to the linear springs at the end of the beams,  $[M_1]$ – $[M_8]$  are the mass matrices,  $\{f\}$  is the generalized load vector. The components of matrices  $[K_{S1}]$ – $[K_{S4}]$  are given here for the clamped–clamped boundary condition, which is the most general situation. These matrices can be constructed for the other boundary conditions considered in this study by choosing appropriate spring constants. It should be noted the size of all matrices in Eq. (A1) is  $N \times N$ . In Eq. (A1), the following abbreviations have been introduced:



$$K_1^{mn} = D_{xx} \int_{-L/2}^{L/2} (x^{m-1})''(x^{n-1})'' dx + k_w \int_{-L/2}^{L/2} (x^{m-1})(x^{n-1}) dx$$

$$m, n = 1, 2, \dots, N \quad (A2)$$

$$K_2^{mn} = -k_w \int_{-L/2}^{L/2} (x^{m-1})(x^{n-1}) dx \quad m, n = 1, 2, \dots, N \quad (A3)$$

$$K_3^{mn} = -B_{xx} \int_{-L/2}^{L/2} (x^{m-1})''(x^{n-1})' dx \quad m, n = 1, 2, \dots, N \quad (A4)$$

$$K_4^{mn} = -k_w \int_{-L/2}^{L/2} (x^{m-1})(x^{n-1}) dx \quad m, n = 1, 2, \dots, N \quad (A5)$$

$$K_5^{mn} = D_{xx} \int_{-L/2}^{L/2} (x^{m-1})''(x^{n-1})'' dx + k_w \int_{-L/2}^{L/2} (x^{m-1})(x^{n-1}) dx$$

$$m, n = 1, 2, \dots, N \quad (A6)$$

$$K_6^{mn} = -B_{xx} \int_{-L/2}^{L/2} (x^{m-1})''(x^{n-1})' dx \quad m, n = 1, 2, \dots, N \quad (A7)$$

$$K_7^{mn} = -B_{xx} \int_{-L/2}^{L/2} (x^{m-1})'(x^{n-1})'' dx \quad m, n = 1, 2, \dots, N \quad (A8)$$

$$K_8^{mn} = A_{xx} \int_{-L/2}^{L/2} (x^{m-1})'(x^{n-1})' dx \quad m, n = 1, 2, \dots, N \quad (A9)$$

$$K_9^{mn} = -B_{xx} \int_{-L/2}^{L/2} (x^{m-1})'(x^{n-1})'' dx \quad m, n = 1, 2, \dots, N \quad (A10)$$

$$K_{10}^{mn} = A_{xx} \int_{-L/2}^{L/2} (x^{m-1})'(x^{n-1})' dx \quad m, n = 1, 2, \dots, N \quad (A11)$$

$$K_{S1}^{mn} = k_{t1}(-L/2)^{m-1}(-L/2)^{n-1} + k_{t2}(L/2)^{m-1}(L/2)^{n-1}$$

$$+ k_{r1}(m-1)(-L/2)^{m-2}(n-1)(-L/2)^{n-2}$$

$$+ k_{r2}(m-1)(L/2)^{m-2}(n-1)(L/2)^{n-2}$$

$$m, n = 1, 2, \dots, N \quad (A12)$$

$$K_{S2}^{mn} = k_{t3}(-L/2)^{m-1}(-L/2)^{n-1} + k_{t4}(L/2)^{m-1}(L/2)^{n-1}$$

$$+ k_{r3}(m-1)(-L/2)^{m-2}(n-1)(-L/2)^{n-2}$$

$$+ k_{r4}(m-1)(L/2)^{m-2}(n-1)(L/2)^{n-2}$$

$$m, n = 1, 2, \dots, N \quad (A13)$$

$$K_{S3}^{mn} = k_{e1}(-L/2)^{m-1}(-L/2)^{n-1} + k_{e2}(L/2)^{m-1}(L/2)^{n-1}$$

$$m, n = 1, 2, \dots, N \quad (A14)$$

$$K_{S4}^{mn} = k_{e3}(-L/2)^{m-1}(-L/2)^{n-1} + k_{e4}(L/2)^{m-1}(L/2)^{n-1}$$

$$m, n = 1, 2, \dots, N \quad (A15)$$

$$M_1^{mn} = I_A \int_{-L/2}^{L/2} (x^{m-1})(x^{n-1}) dx + I_D \int_{-L/2}^{L/2} (x^{m-1})'(x^{n-1})' dx$$

$$m, n = 1, 2, \dots, N \quad (A16)$$

$$M_2^{mn} = -I_B \int_{-L/2}^{L/2} (x^{m-1})'(x^{n-1}) dx \quad m, n = 1, 2, \dots, N \quad (A17)$$

$$M_3^{mn} = I_A \int_{-L/2}^{L/2} (x^{m-1})(x^{n-1}) dx + I_D \int_{-L/2}^{L/2} (x^{m-1})'(x^{n-1})' dx$$

$$m, n = 1, 2, \dots, N \quad (A18)$$

$$M_4^{mn} = -I_B \int_{-L/2}^{L/2} (x^{m-1})'(x^{n-1}) dx \quad m, n = 1, 2, \dots, N \quad (A19)$$

$$M_5^{mn} = -I_B \int_{-L/2}^{L/2} (x^{m-1})(x^{n-1})' dx \quad m, n = 1, 2, \dots, N \quad (A20)$$

$$M_6^{mn} = I_A \int_{-L/2}^{L/2} (x^{m-1})(x^{n-1}) dx \quad m, n = 1, 2, \dots, N \quad (A21)$$

$$M_7^{mn} = -I_B \int_{-L/2}^{L/2} (x^{m-1})(x^{n-1})' dx \quad m, n = 1, 2, \dots, N \quad (A22)$$

$$M_8^{mn} = I_A \int_{-L/2}^{L/2} (x^{m-1})(x^{n-1}) dx \quad m, n = 1, 2, \dots, N \quad (A23)$$

$$f_n = Q(t)(x_Q)^{n-1} \text{ for } 0 \leq t \leq L/v_Q \quad n = 1, 2, \dots, N \quad (A24)$$

$$f_n = 0 \text{ for } t > L/v_Q \quad (A25)$$

where the expressions  $()'$  and  $()''$  are the first and the second derivatives with respect to  $x$ .

## References

- [1] Sankar BV. An elasticity solution for functionally graded beams. *Compos Sci Technol* 2001;61(5):689–96.
- [2] Chakraborty A, Gopalakrishnan S, Reddy JN. A new beam finite element for the analysis of functionally graded materials. *Int J Mech Sci* 2003;45(3):519–39.
- [3] Chakraborty A, Gopalakrishnan S. A spectrally formulated finite element for wave propagation analysis in functionally graded beams. *Int J Solids Struct* 2003;40(10):2421–48.
- [4] Aydogdu M, Taskin V. Free vibration analysis of functionally graded beams with simply supported edges. *Mater Des* 2007;28(5):1651–6.
- [5] Zhong Z, Yu T. Analytical solution of a cantilever functionally graded beam. *Compos Sci Technol* 2007;67(3–4):481–8.
- [6] Ying J, Lü CF, Chen WQ. Two-dimensional elasticity solutions for functionally graded beams resting on elastic foundations. *Compos Struct* 2008;84(3):209–19.
- [7] Kapuria S, Bhattacharyya M, Kumar AN. Bending and free vibration response of layered functionally graded beams: a theoretical model and its experimental validation. *Compos Struct* 2008;82(3):390–402.
- [8] Yang J, Chen Y. Free vibration and buckling analyses of functionally graded beams with edge cracks. *Compos Struct* 2008;83(1):48–60.
- [9] Li XF. A unified approach for analyzing static and dynamic behaviors of functionally graded Timoshenko and Euler–Bernoulli beams. *J Sound Vib* 2008;318(4–5):1210–29.
- [10] Xiang HJ, Yang J. Free and forced vibration of a laminated FGM Timoshenko beam of variable thickness under heat conduction. *Compos Part B: Eng* 2008;39(2):292–303.
- [11] Kadoli R, Akhtar K, Ganesan N. Static analysis of functionally graded beams using higher order shear deformation theory. *Appl Math Model* 2008;32(12):2509–25.
- [12] Benatta MA, Mechab I, Tounsi A, Adda Bedia EA. Static analysis of functionally graded short beams including warping and shear deformation effects. *Comput Mater Sci* 2008;44(2):765–73.
- [13] Sallai BO, Tounsi A, Mechab I, Bachir BM, Meradjah M, Adda BEA. A theoretical analysis of flexional bending of Al/Al<sub>2</sub>O<sub>3</sub> S-FGM thick beams. *Comput Mater Sci* 2009;44(4):1344–50.
- [14] Sina SA, Navazi HM, Haddadpour H. An analytical method for free vibration analysis of functionally graded beams. *Mater Des* 2009;30(3):741–7.
- [15] Şimşek M. Static analysis of a functionally graded beam under a uniformly distributed load by Ritz method. *Int J Eng Appl Sci* 2009;1(3):1–11.
- [16] Pradhan SC, Murmu T. Thermo-mechanical vibration of FGM sandwich beam under variable elastic foundations using differential quadrature method. *J Sound Vib* 2009;321(1–2):342–62.
- [17] Ke LL, Yang J, Kitipornchai S, Xiang Y. Flexural vibration and elastic buckling of a cracked Timoshenko beam made of functionally graded materials. *Mech Adv Mater Struct* 2009;16:488–502.
- [18] Kitipornchai S, Ke LL, Yang J, Xiang Y. Nonlinear vibration of edge cracked functionally graded Timoshenko beams. *J Sound Vib* 2009;324(3–5):962–82.
- [19] Ke LL, Yang J, Kitipornchai S. Postbuckling analysis of edge cracked functionally graded Timoshenko beams under end shortening. *Compos Struct* 2009;90(2):152–60.
- [20] Ke LL, Yang J, Kitipornchai S. Nonlinear free vibration of functionally graded carbon nanotube-reinforced composite beams. *Compos Struct* 2010;92(3):676–83.
- [21] Şimşek M. Fundamental frequency analysis of functionally graded beams by using different higher-order beam theories. *Nucl Eng Des* 2010;240:697–705.
- [22] Kocatürk T, Şimşek M, Akbaş ŞD. Large displacement static analysis of a cantilever Timoshenko beam composed of functionally graded material. *Sci Eng Compos Mater* 2011;18(1):21–34.
- [23] Fallah A, Aghdam MM. Nonlinear free vibration and post-buckling analysis of functionally graded beams on nonlinear elastic foundation. *Eur J Mech A – Solid/A Solids* 2011;30(4):571–83.
- [24] Timoshenko S, Young DH. *Vibration problems in engineering*. New York: Van Nostrand Company; 1955.
- [25] Fryba L. *Vibration of solids and structures under moving loads*. Groningen, The Netherlands: Noordhoff International; 1972.
- [26] Lin YH, Trethewey W. Finite element analysis of elastic beams subjected to moving dynamic loads. *J Sound Vib* 1990;136(2):323–42.
- [27] Lee HP. Dynamic response of a beam with intermediate point constraints subject to a moving load. *J Sound Vib* 1994;171(3):361–8.
- [28] Henchi K, Fafard KM, Dhatt G, Talbot M. Dynamic behavior of multi-span beams under moving loads. *J Sound Vib* 1997;199(1):33–50.
- [29] Wang RT. Vibration of multi-span Timoshenko beams to a moving force. *J Sound Vib* 1997;207(5):731–42.
- [30] Zheng DY, Cheung YK, Au FTK, Cheng YS. Vibration of multi-span non-uniform beams under moving loads by using modified beam vibration functions. *J Sound Vib* 1998;212(3):455–67.
- [31] Zhu XQ, Law SS. Moving force identification on multi-span continuous bridge. *J Sound Vib* 1999;228(2):377–96.
- [32] Abu-Hilal M, Mohsen M. Vibration of beams with general boundary conditions due to moving harmonic load. *J Sound Vib* 2000;232(4):703–17.

- [33] Michaltsos GT. Dynamic behaviour of a single-span beam subjected to loads moving with variable speeds. *J Sound Vib* 2002;258(2):359–72.
- [34] Dugush YA, Eisenberger M. Vibrations of non-uniform continuous beams under moving loads. *J Sound Vib* 2002;254(5):911–26.
- [35] Abu-Hilal M. Vibration of beams with general boundary conditions due to a moving random load. *Arch Appl Mech* 2003;72(9):637–50.
- [36] Garinei A. Vibrations of simple beam-like modelled bridge under harmonic moving loads. *Int J Eng Sci* 2006;44(11–12):778–87.
- [37] Kocatürk T, Şimşek M. Vibration of viscoelastic beams subjected to an eccentric compressive force and a concentrated moving harmonic force. *J Sound Vib* 2006;291(1–2):302–22.
- [38] Kocatürk T, Şimşek M. Dynamic analysis of eccentrically prestressed viscoelastic Timoshenko beams under a moving harmonic load. *Comput Struct* 2006;84(31–32):2113–27.
- [39] Şimşek M, Kocatürk T. Dynamic analysis of an eccentrically prestressed damped beam under a moving harmonic force using higher order shear deformation theory. *ASCE J Struct Eng* 2007;133(12):1733–41.
- [40] Şimşek M, Kocatürk T. Nonlinear dynamic analysis of an eccentrically prestressed damped beam under a concentrated moving harmonic load. *J Sound Vib* 2009;320(1–2):235–53.
- [41] Yang J, Chen Y, Xiang Y, Jia XL. Free and forced vibration of cracked inhomogeneous beams under an axial force and a moving load. *J Sound Vib* 2008;312(1–2):166–81.
- [42] Şimşek M, Kocatürk T. Free and forced vibration of a functionally graded beam subjected to a concentrated moving harmonic load. *Compos Struct* 2009;90(4):465–73.
- [43] Khalili SMR, Jafari AA, Eftekhari SA. A mixed Ritz-DQ method for forced vibration of functionally graded beams carrying moving loads. *Compos Struct* 2010;92:2497–511.
- [44] Şimşek M. Vibration analysis of a functionally graded beam under a moving mass by using different beam theories. *Compos Struct* 2010;92(4):904–17.
- [45] Şimşek M. Non-linear vibration analysis of a functionally graded Timoshenko beam under action of a moving harmonic load. *Compos Struct* 2010;92:2532–46.
- [46] Yan T, Kitipornchai S, Yang J, He XQ. Dynamic behaviour of edge-cracked shear deformable functionally graded beams on an elastic foundation under a moving load. *Compos Struct* 2011;93(11):2992–3001.
- [47] Oniszczuk Z. Free transverse vibrations of elastically connected simply supported double-beam complex system. *J Sound Vib* 2000;232(2):387–403.
- [48] Aida T, Toda S, Ogawa N, Imada Y. Vibration control of beams by beam-type dynamic vibration absorbers. *J Eng Mech* 1992;118(2):248–58.
- [49] Hussein MFM, Hunt HEM. Modelling of floating-slab tracks with continuous slabs under oscillating moving loads. *J Sound Vib* 2006;297:37–54.
- [50] Shamalta M, Metrikine AV. Analytical study of the dynamic response of an embedded railway track to a moving load. *Arc Appl Mech* 2003;73:131–46.
- [51] Kelly SG, Srinivas S. Free vibrations of elastically connected stretched beams. *J Sound Vib* 2009;326:883–93.
- [52] Seelig JM, Hoppmann II WH. Normal mode vibrations of systems of elastically connected parallel bars. *J Acoust Soc Am* 1964;36(1):93–9.
- [53] Kessel PG. Resonances excited in an elastically connected double-beam system by a cyclic moving load. *J Acoust Soc Am* 1966;40(3):684–7.
- [54] Rao SS. Natural vibrations of systems of elastically connected Timoshenko beams. *J Acoust Soc Am* 1974;55(6):1232–7.
- [55] Chonan S. Dynamical behaviours of elastically connected double-beam systems subjected to an impulsive load. *Bull JSME* 1976;19(132):595–603.
- [56] Vu HV, Ordonez AM, Karnopp BH. Vibration of a double-beam system. *J Sound Vib* 2000;229(4):807–22.
- [57] Oniszczuk Z. Forced transverse vibrations of an elastically connected complex simply supported double-beam system. *J Sound Vib* 2003;264:273–86.
- [58] Abu-Hilal M. Dynamic response of a double Euler-Bernoulli beam due to a moving constant load. *J Sound Vib* 2006;297:477–91.
- [59] Zhang YQ, Lu Y, Wang SL, Liu X. Vibration and buckling of a double-beam system under compressive axial loading. *J Sound Vib* 2008;318:341–52.
- [60] Zhang YQ, Lu Y, Ma GW. Effect of compressive axial load on forced transverse vibrations of a double-beam system. *Int J Mech Sci* 2008;50:299–305.
- [61] Jun L, Hongxing H. Dynamic stiffness vibration analysis of an elastically connected three-beam system. *Appl Acoust* 2008;69:591–600.
- [62] Jun L, Yong C, Hongxing H. Exact dynamic stiffness matrix of a Timoshenko three-beam system. *Int J Mech Sci* 2008;50:1023–34.
- [63] Ariei A, Ziaei-Rad S, Ghayour M. Transverse vibration of a multiple-Timoshenko beam system with intermediate elastic connections due to a moving load. *Arch Appl Mech* 2011;81:263–81.
- [64] Şimşek M. Nonlocal effects in the forced vibration of an elastically connected double-carbon nanotube system under a moving nanoparticle. *Comput Mater Sci* 2011;50(7):2112–23.
- [65] Palmeri A, Adhikari S. A Galerkin-type state-space approach for transverse vibrations of slender double-beam systems with viscoelastic inner layer. *J Sound Vib* 2011;330:6372–86.
- [66] Newmark NM. A method of computation for structural dynamics. *ASCE Eng Mech Div* 1959;85:67–94.
- [67] Wakashima K, Hirano T, Niino M. Space applications of advanced structural materials. *ESA* 1990;SP:303–97.